X-ray emission from accreting Black Holes

Fernando Eugenio Barrio Madias

Master of Science Thesis

Department of Physics

University of Durham

DURHAM - JANUARY 2003

to all the ones
who helped and supported
this achievement.

Abstract

X-ray emission from accreting Black Holes.

Fernando Eugenio Barrio Madias[1]
Department of Physics, University of Durham.

In this thesis I use state of the art models of x-ray emission from accreting black holes in order to observationally constrain the accretion geometry. The broad-band RXTE PCA and HEXTE spectrum of Cyg X-1 from $3 - 200keV$ is fit with reflection models which calculate the vertical ionization structure of an x-ray illuminated disc. Two geometries were considered corresponding to a truncated disc/inner hot flow and magnetic flares above an untruncated disc. Both models are able to fit the PCA $3 - 20keV$ data, but with very different spectral components. In the magnetic flare models the $3 - 20keV$ PCA spectrum contains a large amount of highly ionized reflection while in the truncated disc models the amount of reflection is rather small. The Compton downscattering rollover in the reflected emission means that the magnetic flare models predict a break in the spectrum at the high energies covered by the HEXTE bandpass which is *not* seen. By contrast the weakly illuminated truncated disc models can easily fit the $3 - 200keV$ spectra, strongly suggesting that this is the preferential geometry of galactic black hole binaries in the hard/low state.

[1]eugenio.barrio@durham.ac.uk

Contents

List of Figures

Declaration

This is a dissertation submitted to the University of Durham in accordance with the regulations for admission to the degree of Master of Science.

The work presented in this thesis was undertaken whilst the Author was a graduate student working in the Department of Physics at the University of Durham under the supervision of Dr. Chris Done. The majority of this work is the authors own but some work presented in this thesis was carried out in close collaboration with Dr. Done.

The observational work shown in this thesis made use of data obtained through the High Energy Astrophysics Science Archive, provided by the NASA Goddard Space Flight Center.

Some of the material in this thesis appears in Barrio et al. 2003.

While in Durham the author was a member of Ustinov College (Graduate Society), University of Durham.

Chapter 1

Black Holes

Cuánto mejor es morir por algo que vivir por nada.

Anónimo

Black Holes do exist. They were first a theoretical prediction, a mind game of how extreme a gravitational field could be. The ultimate collapsed object, a trap not even light can escape from. Not surprisingly this utterly extreme concept acquired notoriety far outside the science community, mystically linked to Einstein's GR, outer space, space-time, higher dimensions, time travel and science fiction.

By definition they are not observable (no information can escape from within a black hole), but their extraordinary gravitational force can perturb their surroundings in a measurable way. Nowadays black holes are key elements in stellar and galactic evolutionary models.

In this chapter the concept of black holes is introduced, along with ways of classifying them, and their observed behavior.

1.1 Introduction

The very first idea closely related to what we now call a black hole was introduced in 1783 by the English astronomer and clergyman John Michell as 'dark stars'. Following Newton's gravitational theory as underlined in his Principia, Michell worked out the size the sun should have for its escape velocity to be equal to the speed of the light, giving a necessary condition for a star not to be seen. The same calculations were independently achieved not much later by the French mathematician Pierre-Simon Laplace. Laplace thought that a black star was a crazy idea and discontinued his work.

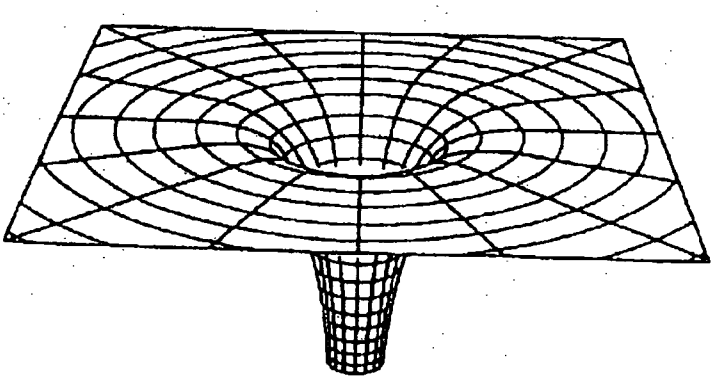

Figure 1.1: Extreme warping of space-time around a black hole.

More than a century later, based on a new gravitation theory: Einstein's General Theory of Relativity, Karl Schwarzschild assessed the problem from a much accurate perspective. He found, in 1916, a solution of Einstein's equations corresponding to the simplest black hole namely Schwarzschild metric (fig. 1.1).

The Schwarzschild metric, relating space-time intervals in a static spherical symmetric gravitational field in the empty space-time surrounding some massive spherical object like a star is

$$c^2\,dt^2 = \left(1 - \frac{2GM}{c^2 r}\right) c^2 dt^2 - \left(1 - \frac{2GM}{c^2 r}\right)^{-1} dr^2 - r^2\,d\theta^2 - r^2 \sin^2\theta\,d\phi^2 \qquad (1.1)$$

A new field in Physics was born, developed by many great names in science like Ricci, Hilbert, Oppenheimer, Friedman, Wheeler (who, in 1970s, coined the name 'black hole'), Kerr, and Hawking among many others.

Black Holes

The Schwarzschild metric predicts a surface from which light can not escape, the 'Event Horizon', a globally defined null surface. All the events beyond the Schwarzschild radius, $R_s = \frac{2GM}{c^2}$, are disconnected from the rest of the universe, so the horizon forms a border where no information can reach us. We can never *see* directly (at any frequency), a black hole.

At the centre of the event horizon surface there is a mathematical singularity, a place where the known laws of physics are no longer valid, and any kind of speculation is equally plausible, like worm holes (a hole in the space-time web connecting two otherwise distant regions). All the mass of the black hole is compressed to a single point of infinite density. To understand this region a quantum gravity theory has to be developed. This theory

would be able to reconcile General Relativity (how gravity, and space geometry relates) with Quantum Physics (the processes on extremely small scales).

Such quantum theories of gravity are an active field of research nowadays, but this is not the path followed in this work.

1.2 Thinking of Black Holes

There are three main size ranges of black holes: stellar mass black holes made from the collapsing core of a massive star, supermassive black holes at a center of galaxies, and miniature black holes believed to be created in the early universe during inflation.

Stellar Black Holes:

In order of understanding the birth of a black hole, one must first understand the life cycle of a star: A star is created when a cloud of gas, mainly hydrogen, some helium and traces of other heavier elements, begins to collapse into itself under its own gravity. The gas heated by the gravitational energy release eventually reaches high enough temperatures in its core so that nuclear fusion reactions can begin. The heat makes the internal pressure rise, stopping the contraction. These two forces balance, and the proto-star becomes a stable main sequence star.

When a massive star burns out most of its hydrogen fuel in the core, it follows a complex evolutionary path, fusing progressively heavier and heavier elements, culminating in iron. Iron is the heaviest element can be stably synthesized in the core of stars, as it is the heaviest element for which fusion *releases* binding energy.

The iron builds up in the core, held up by electron degeneracy pressure. When the mass of the core reaches the Chandrasekar limit of about $1.4M_{\odot}$, then the electron degeneracy pressure can not hold the weight of the star any longer. Electrons recombine with the protons and create neutrons. The size of the core reduces from about 10^4 km (approximately the size of the Earth) to 10 km in diameter, held up by neutron degeneracy pressure. While gravity still acting, the outer layers of the star start to collapse. This violent accretion generates a supernova explosion, which blows away of the outermost layers of the star.

Depending on its mass, the core may stay as neutron star or collapse further into a black hole.

Supermassive Black Holes:

Current models of galaxy formation suggest that the very first stars (gigantic balls of hydrogen and helium with almost no heavier elements) formed in the place where later galaxies would grow. These very old stars possibly ended as black holes, but then accreted much more material from their surroundings: interstellar medium, molecular clouds, merging with other stars or black holes, etc. This merging/accreting mechanism leads to a wide range of masses from $\sim 10^4 - 10^9 M_\odot$. These are the objects believed to be at the centre of most galaxies, also the ones which power active galactic nuclei (AGNs), radio galaxies, and quasi stellar objects (QSOs), (see e.g. the review by Kormendy & Gebhardt 2001).

Mini Black Holes:

Inflationary cosmological theories abound for the existence of mini black holes, perhaps formed shortly after the Big Bang.

Some particle physicist also claim that the TeV physics that they will shortly be able to test in the next generation of colliders may produce mini black holes. If mini black holes can be produced during particle collisions in laboratories, it is also possible for them to be created in a cosmic ray collision, although this seems unlikely (Hossenfelder et al. 2002)

For such mini black holes Hawking Radiation might be important: Purely theoretically it was concluded that a black hole must emit some sort of radiation, because it *must* have some kind of entropy, so must emit energy. In September 1973, J. Zeldovitz and A. Strovinski, showed that every spinning black hole must emit radiation and particles. It emits energy and particles as if it were a black body with a temperature depending only on its mass: the more massive it is, the cooler it gets. In November 1973, Stephen Hawking, added some calculations, and found out that also a non-spinning black hole should emit energy and particles. The mechanism can be described as creating a particle/antiparticle pair in the vicinity of a black hole, the particle is more likely to escape and the antiparticle to get trapped by the event horizon, i.e. be annihilated by a particle from the black hole. For the external observer is like a particle is coming from the black hole, this is called 'Hawking Radiation'. This effect could cause black holes to evaporate. The calculations also show that the time required for the evaporation would depend upon the mass of the black hole. Very massive black holes would need a time that is much longer than the current age of the universe. Only miniature black holes are thought to be capable of evaporation within the existing time of our universe. For a black hole formed at the time

of the Big Bang to evaporate today its mass must be about $10^{5-12}g$, (Hamilton 1998).

General Relativity also predicts that a black hole in orbit (accelerated) must emit gravitational waves. The scenario for this to happen may be two black holes orbiting each other as a binary system, and radiating more gravitational waves as they get closer until they merge. Gravitational waves experiments such as LIGO (and the future space based LISA) plan to detect such signals of merging black holes.

However, these two direct ways to detect black holes (Hawking radiation and gravitational waves) are currently not possible. To study black holes we have to use more indirect methods, by looking at the effects of the black holes gravity on nearby material.

1.3 Observing Black Holes

The first attempt to combine black holes with observed sources came after the discoveries of quasars, radio pulsars and compact x-ray sources in late 1960s. This was only possible due to the development of radio and x-ray astronomy. Most of the newly discovered x-ray sources showed two very particular characteristics: large amounts of x-ray emission with high variability on all time-scales.

This rapid variability on milliseconds time-scales suggested that they were very small objects, since the size of the source restricts the typical variability time-scale to be less than the light travel time across the source. In 1971 Oda et al. were the first to suggest that Cyg X-1 could be a black hole binary, on the basis of its peculiar characteristics, including in particular the rapid x-ray variability on time-scales of a few hundred of seconds down to milliseconds.

The high x-ray luminosity observed from a very small region requires a very effective mechanism for energy release, showing that these sources were not ordinary stars with ordinary nuclear reactions at their core. Conversion of gravitational energy into radiation becomes the only plausible explanation for such bright objects.

Binary Systems

Observations of binary systems when one of the two stars is invisible cannot lead to the conclusion that the invisible star is a black-hole, because it may also be a faint star, or there may be some other reason for it being 'invisible' from our point of view. But if accompanied by observations of high x-ray emission, the most reasonable explanation is that these are formed because of matter falling from the visible star to the invisible object.

The first x-ray binary was optically identified in the late 60s as Sco X-1 followed by many others like Cyg X-1, Her X-1, Cen X-3, etc. The search for the optical counterparts and the analysis of the orbital periods favored the model in which the invisible companion was a compact object i.e. a neutron star or a black hole.

The only way to be sure about whether it is a black hole or not is through dynamical mass determination. There is a limit of $\sim 3M_{\odot}$ for the maximum mass of a neutron star. Above this limit the object collapses inevitably to a black hole. But this orbital analysis is not always possible as the companion star may be faint.

But happily there are some important differences to spot. Neutron stars may have strong magnetic fields, which can distort the accretion process. The accreting flow instead follows the field lines so that the accretion takes place onto the poles showing, as the star rotates, x-ray pulses. Also, contrary to black holes, neutron stars have a solid surface so the accreting material builds upon this surface and can eventually give rise to hydrogen or helium fusion, causing x-ray bursts. Both these are clear distinguishing signals of a neutron star primary, but not seeing these signals is not an unambiguous signature of a black hole.

It is believed the most of the stars are in binary systems, and most of them have mass transfer at some point of their evolution. In the special case in which one is a compact object, the companion star can lose material into the principal gravitational potential through a stellar wind. It also can happen that when the separation contracts due to loss of angular momentum (by tidal forces, gravitational waves or mass ejection), then the accretion proceeds through Roche Lobe Overflow.

In order to understand how the gas moves from one star into the gravitational potential of the other, we will follow the Roche problem.

Roche Lobe Overflow

In a binary system two stars orbit each other in Keplerian orbits. The Roche lobe of each star is each one of the lobes in the eight-like critical equipotential surface of the Roche potential (fig. 1.2):

$$R(r) = -\frac{GM_1}{|\mathbf{r}-\mathbf{r_1}|} - \frac{GM_2}{|\mathbf{r}-\mathbf{r_2}|} - \frac{1}{2}\left(\omega \bigwedge \mathbf{r}\right)^2 \tag{1.2}$$

where $\mathbf{r_1}$ $\mathbf{r_2}$ are the position vectors of the stars and $M_1 M_2$ their respective masses, and assuming circular orbits. The centre of reference is their common centre of mass, rotating with angular velocity

$$\omega = \left[\frac{(M_1+M_2)}{(M_2/M_1)^3}\right]^{1/2} \mathbf{e} \tag{1.3}$$

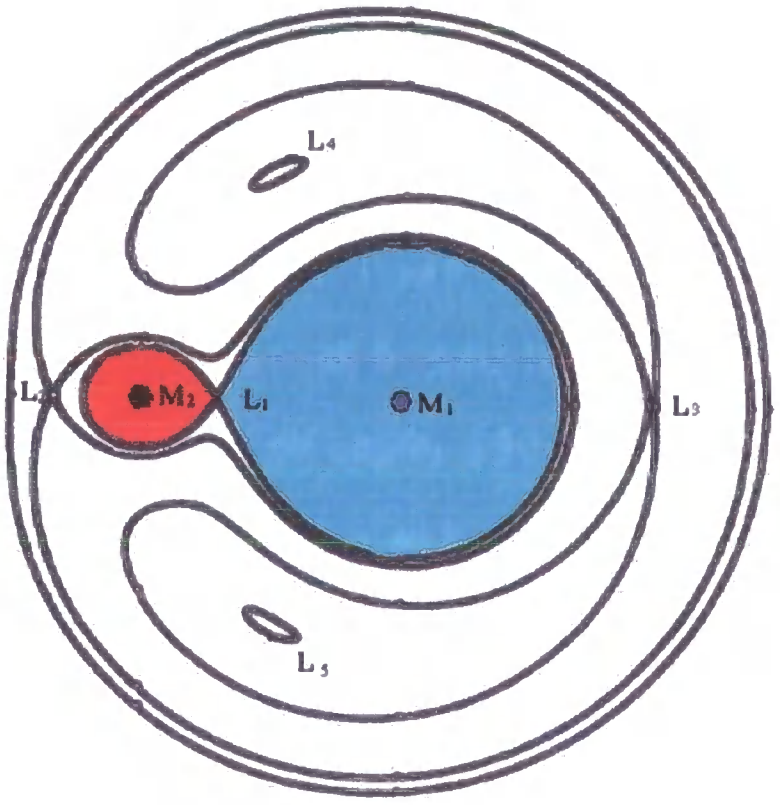

Figure 1.2: The Roche Lobe diagram. $L_i, i = 1, 2, ...$ are the Lagrangian points 1, 2, etc. (Koji Mukai homepage).

When the separation shrinks (due to loss of angular momentum), and/or the companion star evolves and expands, the star fills its Roche lobe and material falls through the inner Lagrangian point L_1, to the compact object lobe.

This material has some finite angular momentum, which it has to lose in order to be accreted. The most plausible way is through forming an accretion disk. While orbiting in the accretion disc, the gas follows Keplerian orbits, where internal magnetic shear (Balbus & Hawley 2002; and references therein) between differentially rotating ring of gas, transports the angular momentum outwards, letting the material fall into a closer orbit.

1.4 Disc Accretion

The material accreting onto a compact object has to lose angular momentum to reach the surface/event horizon. The simplest scenario is a gaseous disc in hydrostatic equilib-

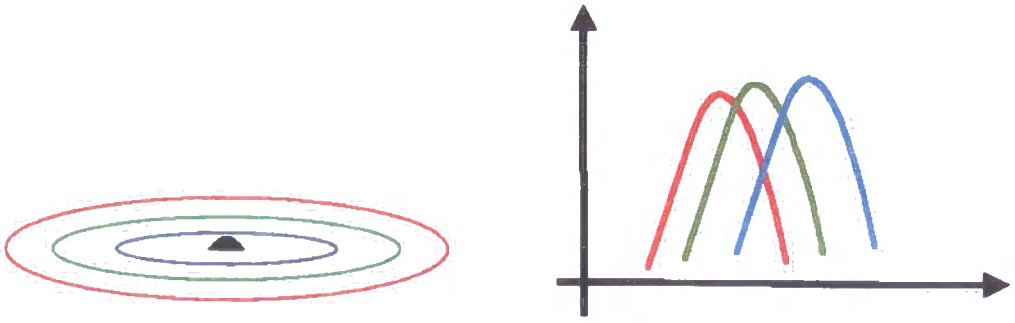

Figure 1.3: Part a. shows differentially rotating orbit velocity at different radii; while part b the multicolour black body schematic emission from different parts of the disc.

rium with Keplerian orbit around a black hole in which accretes at a constant rate. The disc temperature depends on the radius. A first estimate can be made from energy conservation conditions, with half of the potential energy radiated in each differential orbit ring as a blackbody spectrum:

$$\frac{GM\dot{M}}{2r^2}\,dR = 2\pi R\,dR\,\sigma T^4 \tag{1.4}$$

$$T = \left(\frac{GM\dot{M}}{4\pi\sigma}\right)^{1/4} R^{-3/4} \tag{1.5}$$

where G the gravitational constant, M the mass of the central object, $\dot{M}$ is the accretion rate, and σ is the Stephan-Boltzmann constant.

A more accurate view, taking into account the shear stress on the disc, gives:

$$T = \left[\frac{3GM\dot{M}}{8\pi\sigma R^3}\left(1-\sqrt{\frac{R_{in}}{R}}\right)\right]^{1/4} \tag{1.6}$$

This is not dependent on the form of the viscosity, as it simply depends on the energetic of the orbits.

The total spectrum from the disc will be the sum of all these temperatures from the innermost radius to the outer edge. These gives a multicolour black body spectrum peaking at $\sim 1keV$ for stellar mass black holes accreting at close to the Eddington limit; while for AGNs (with larger $M\dot{M}$) the typical temperature are around $10eV$ (fig. 1.3).

The first solution of the full accretion flow equations was developed by Shakura and Sunyaev (hereafter SS) in 1973. It assumes that the gravitational energy is radiated locally, and it produces a geometrically thin disc structure. The basic SS set of equations is as follows:

$$\dot{M} = -2\pi R v_r \Sigma$$

$$
\begin{aligned}
\Omega_K &= \sqrt{\frac{GM}{R^3}} \\
\nu\Sigma &= \frac{1}{3\pi}\dot{M}\left(1-\sqrt{\frac{R_{in}}{R}}\right) \\
H &= \frac{c_s}{\Omega_K} \\
\frac{9}{4}\nu\Sigma\Omega_K^2 &= \frac{8acT_c^4}{3\tau}, \qquad a = 4\sigma c_{SB}^{-1} \\
p &= \frac{2\rho k_B T_c}{m_H} + \frac{aT_c^4}{3} \\
\Sigma &= 2\rho H \\
c_s &= \left(\frac{p}{\rho}\right)^{\frac{1}{2}} \\
\tau &= \frac{1}{2}\overline{\kappa}\Sigma \\
\overline{\kappa} &= \kappa_{es} + \kappa_0 \rho T_c^{-3.5}
\end{aligned}
$$

These are 10 equations for 11 unknowns namely radial velocity v_r, surface density Σ, Keplerian frequency Ω_K, Height H (as measured from the centre of the disc), mass density ρ, kinetic viscosity ν, sound speed c_s, total pressure p $(= p_{gas} + p_{rad})$, central temperature T_c, and opacity $\overline{\kappa}$ $(= \kappa_{es} + \kappa_{ff}$, i.e. the sum of electron scattering and free-free opacity) in terms of R, M, and $\dot{M}$.

To solve this set of equations requires another relation between these quantities, which determines the viscosity stress. The key insight of SS was that our ignorance about the nature of the turbulent shear viscosity could be incorporated into a single parameter α:

$$\frac{3}{2}\rho\nu\Omega_K = \alpha p \qquad (= -t_{r\varphi}) \tag{1.7}$$

This SS set of equations can be solved numerically, but can also be solved analytically for a few special cases. The three original cases identified by SS, consist of three regions at different radii (and by eq. 1.6, different temperatures). The results are presented in terms of the following dimensionless quantities:

$$m = \frac{M}{M_\odot}, \qquad \dot{m} = \frac{\dot{M}}{\dot{M}_{crit}}, \qquad r = \frac{R}{R_s}, \qquad f = 1 - \sqrt{\frac{3R_s}{R}}, \qquad \text{and} \qquad \alpha \tag{1.8}$$

where

$$\dot{M}_{crit} = \frac{L_E}{c^2} = \frac{4\pi cGMm_H}{\sigma_T} \tag{1.9}$$

i.e. the critical mass-flow rate that would give the Eddington luminosity L_E, for complete conversion efficiency of mass to radiation. For a standard Schwarzschild black hole efficiency $\eta = 0.067$, so L_E corresponds to $\dot{m} = 15$.

A) Inner disc

The temperature and density are high so that the radiation pressure dominates over the gas pressure, and the free-free opacity is negligible compared to electron scattering opacity.

$$\begin{aligned} H &= 5.5 \times 10^4 m\dot{m} f \; cm \\ \rho &= 9.0 \times 10^{-4} \alpha^{-1} m^{-1} \dot{m}^{-2} r^{3/2} f^{-2} \; gcm^{-3} \\ T_c &= 4.9 \times 10^7 \alpha^{-1/4} m^{-1/4} r^{-3/8} \; K \end{aligned}$$

B) Middle disc

Temperature and density drops, we approximate total pressure to gas pressure but still the free-free opacity is very much less than the electron scattering.

$$\begin{aligned} H &= 2.7 \times 10^3 \alpha^{-1/10} m^{9/10} \dot{m}^{1/5} r^{21/20} f^{1/5} \; cm \\ \rho &= 8.0 \alpha^{-7/10} m^{-7/10} \dot{m}^{2/5} r^{-33/20} f^{2/5} \; gcm^{-3} \\ T_c &= 2.2 \times 10^8 \alpha^{-1/5} m^{-1/5} \dot{m}^{2/5} r^{-9/10} f^{2/5} \; K \end{aligned}$$

C) Outer disc

Density and temperature are low, therefore $p \sim p_{gas}$, and $\overline{\kappa} \sim \kappa_{ff}$

$$\begin{aligned} H &= 1.5 \times 10^3 \alpha^{-1/10} m^{9/10} \dot{m}^{3/20} r^{-9/8} f^{3/20} \; cm \\ \rho &= 4.7 \times 10 \alpha^{-7/10} m^{-7/10} \dot{m}^{11/20} r^{-15/8} f^{11/20} \; gcm^{-3} \\ T_c &= 6.9 \times 10^7 \alpha^{-1/5} m^{-1/5} \dot{m}^{3/10} r^{-3/4} f^{3/10} \; K \end{aligned}$$

Such accretion disc models show that energy can be extracted by material falling onto a black hole. In the next chapter we compare the predictions of these disc models into the observed spectra from accreting black holes.

Chapter 2

X-Rays from Black Holes

I ask you to look both ways.
For the road to a knowledge of the stars leads through the atom;
and important knowledge of the atom has been reached
through the stars.

Sir Arthur Eddington

From observations of the spectra it was found that binary systems have two (sometimes more) distinct states: the hard/low state and the soft/high state. These changes of states are believed to be correlated with the mass accretion rate $\dot{m}$.

The hard/low state is characterized by a hard power law with photon index ($\Gamma \sim 1.5 - 1.9$), peaking at $\sim 100keV$ and rolling over at higher energies. The soft/high state peaks at a few keV but has a steep power law tail ($\Gamma \sim 2.0 - 2.5$), which extents out to $E > 511keV$ (fig. 2.1).

However, a multicolour disc black body spectra expected from the accretion disc is not able to produce the hard x-rays observed. Theses hard x-rays should come from somewhere else other than the disc. Variability data shows the hard x-rays source must be small, yet it also has to be energetically dominant, so probably is close to the central object. The main idea is that hot electrons in a low density (optically thin) environment upscatter the thermal emission from the disc up to x-ray energies. This process is know as Compton Scattering.

2.1 Compton Scattering

In 1923 A. Compton discovered that the wavelength of hard x-ray radiation increases when it is scattered from stationary electron. In a more general case, depending on the

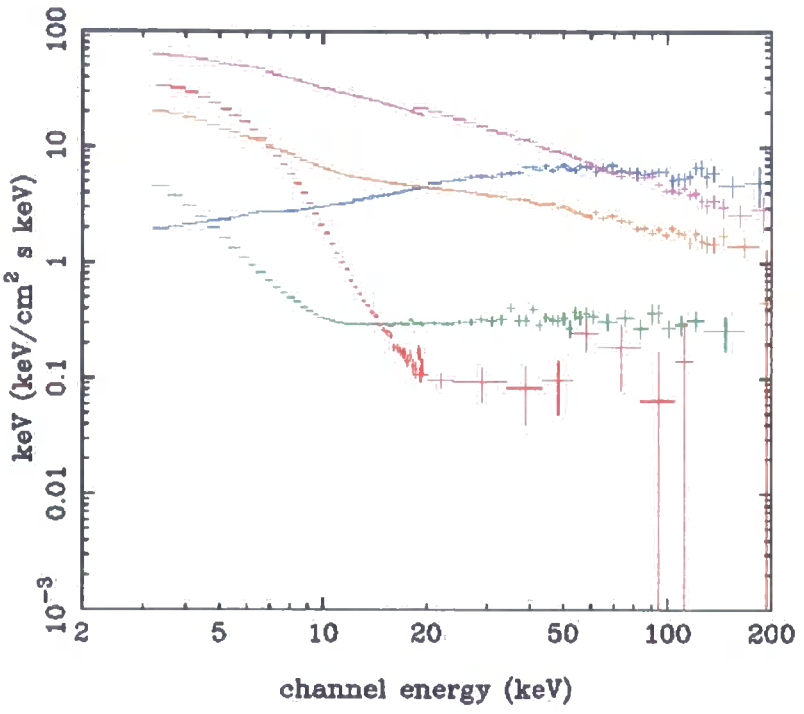

Figure 2.1: Hard to soft to ultra-soft transition of spectra state of a black hole J1550-564.

relative energy of the photons and electrons, this can result in downscattering when the photon loses energy, or upscattering when the photon gains energy.

An electron with velocity parameter $\beta = v/c$ in the direction $\mathbf{n_e}$ and total energy $\gamma m_e c^2$, collides with a photon of energy $E_i = h\nu_i$ in the direction $\mathbf{n_i}$. After the interaction the photon has direction $\mathbf{n_o}$, with energy $E_o = h\nu_o$ where

$$\frac{E_o}{E_i} = \frac{1 - \beta \mathbf{n_i}.\mathbf{n_e}}{[1 - \beta \mathbf{n_o}.\mathbf{n_e} + (E_i/\gamma m_e c^2)\,(1 - \mathbf{n_i}.\mathbf{n_o})]} \tag{2.1}$$

There is a fundamental limit to the output energy of the photon know as the Kein Nishima limit, which is the total energy of the system before the scattering (the photon can not gain more energy than there is in the system).

This formula can be simplified for a few special cases (see e.g. Longair, or Rybicki & Lightman):

A) Downscattering

When the electron speed is low $\beta \to 0$ and $\gamma \to 1$ (e.g. $\beta \ll E_i/m_e c^2$) the electron recoils when hit by the photon, the photon loses energy and is downscattered.

$$\frac{E_o}{E_i} = \frac{1}{1 + (E_i/m_e c^2)\,(1 - \mathbf{n_i}.\mathbf{n_o})} \tag{2.2}$$

or

$$\frac{\Delta E}{E_i} \approx -\frac{E_i}{m_e c^2} \qquad \ll 1 \tag{2.3}$$

B) Inverse Compton Scattering or upscattering(in the Thompson limit)

If the electron is moving with a high velocity, then the relativistic transformations dominate and the energy is

$$\frac{E_o}{E_i} = \frac{(1 - \beta \mathbf{n_i}.\mathbf{n_e})}{(1 - \beta \mathbf{n_o}.\mathbf{n_e})} \tag{2.4}$$

in the Thomson limit $\gamma E_i \ll m_e c^2$, (i.e. when the electron recoil in the rest frame is small).

We now consider an isotropic photon field with energy density U_{rad} at a single energy E_i. The energy loss rate, averaged over angle is

$$\frac{dE}{dt} = \frac{4}{3}\sigma_T c U_{rad}\left(\gamma^2 - 1\right) \tag{2.5}$$

where σ_T is the Thompson cross section (valid for low photon energies).

The number of photons scattered per unit of time

$$\frac{dN}{dt} = \frac{\sigma_T c U_{rad}}{E_i} \tag{2.6}$$

so the average energy

$$\frac{dE/dt}{dN/dt} = \frac{4}{3}\left(\gamma^2 - 1\right) E_i \tag{2.7}$$

as $\beta \to 0$, so $\gamma \to 1$

$$\frac{dE/dt}{dN/dt} \approx \frac{4}{3}\beta^2 E_i \tag{2.8}$$

For a upscattering off a thermal distribution of electrons,

$$\frac{1}{2} m_e \mathrm{v}^2 = \frac{3}{2}\mathrm{kT} \tag{2.9}$$

the average electron velocity gives

$$\beta^2 = 3kT/m_e c^2 \tag{2.10}$$

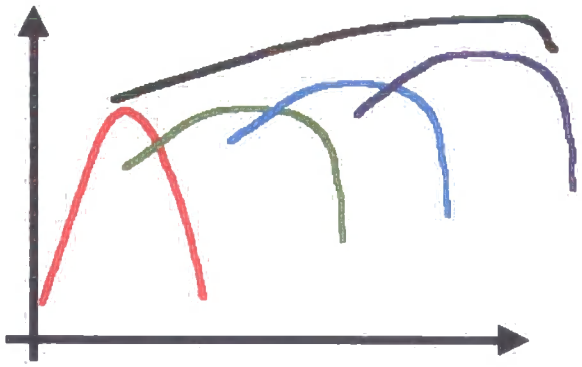

Figure 2.2: This schema shows how multiple Compton scattering can buit up a broad spectrum caracterized with a power law tail with rollover at $\sim \theta_e$. It is $log\ \nu f_\nu$ in the ordinates, and $log\ \nu$ in the abscissas.

so the average energy boost becomes

$$\frac{dE/dt}{dN/dt} \approx \frac{4kT_e}{m_e c^2} E_i \tag{2.11}$$

or

$$\frac{\Delta E}{E_i} \approx 4\theta, \qquad \theta = \frac{kT_e}{mc^2} \ll 1 \tag{2.12}$$

Upscattering and downscattering can be combined together to give

$$\frac{\Delta E}{E} \approx 4\theta - \frac{E_i}{m_e c^2} \tag{2.13}$$

so if the electron temperature $\theta \gg \frac{E_i}{m_e c^2}$, then upscattering dominates.

The optical depth can be computed as

$$\tau = n\sigma_T R \tag{2.14}$$

i.e. is proportional to the number density of electrons n. For $\tau \gg 1$ (optically thick material), the photons scatters many times before escaping. A random walk shows that a typical number of scatterings is τ^2.

The illuminating beam will receive a boosts of energy by 4θ for each scattering, forming a spectra from multiple scatterings. Multiple Compton scattering will lead to the power law tail extending to hard x-ray energies (see fig. 2.2).

Figure 2.3: Scheme of the current geometry models for accretion discs around stellar mass black holes. In part a. magnetic flares model and in part b. the truncated disc/hot inner flow geometry.

2.2 A Geometry Problem

There is no consensus on the geometry of this hot region that produces the observed x-rays. There are currently two main models, one in which the hot electrons are confined in magnetic flares above a disc which extends down to the last stable orbit around the black hole (magnetic flares), and one in which the electrons form a quasi spherical hot flow, replacing the inner disc (truncated disc) see fig. 2.3.

The magnetic flare model is motivated by the discovery that the physical mechanism for the disc viscosity is a magneto hydrodynamic dynamo (e.g. the review by Balbus & Hawley 2002). Buoyancy could cause the magnetic field loops to rise up to the surface of the disc, so they can reconnect in regions of fairly low particle density, forming a patchy corona. Numerical simulations (although these are highly incomplete as in general the simulated discs are not radiative) do show this happening (Hawley 2000), but they do not yet carry enough power to reproduce the observed low/hard state (Miller & Stone 2000).

The truncated disc model has its physical basis in the accretion flow equations. The standard Shakura-Sunyaev disc solution assumes that the accreting material is at one temperature (protons and electrons thermalize) and that the accretion energy released by viscosity is radiated efficiently. At low mass accretion rates neither of these are necessarily true. The thermalization time-scale between the electrons and protons can be long, so the flow is intrinsically a two temperature plasma. Where the electrons radiate most of the gravitational energy through comptonization of photons from the outer disc then the structure of the hot inner flow is given by Shapiro, Lightman & Eardley (1976). Alternatively, if the protons carry most of the accretion energy into the black hole then this forms the advection dominated accretion flows (ADAF) (Narayan & Yi 1995). These are related, as in general both advection and radiative cooling are important for a hot accretion flow (Chen et al. 1995, Zdziarski 1998).

In order to truly understand the accretion processes, this geometry dilemma has to be solved. This is the aim of the present thesis. We try to model the disc structure in the two geometries described above, and compare them against observations to determine which of the geometry models is more plausible. Hopefully later, this ideas may be extended to the AGNs and QSOs.

Chapter 3

Irradiated Accretion Discs

You can know the name of a bird in all the languages of the world, but when you're finished, you'll know absolutely nothing whatever about the bird... So let's look at the bird and see what it's doing - that's what counts. I learned very early the difference between knowing the name of something and knowing something.

Richard Feynman

In chapter one we reviewed that a stable disc in hydrostatic equilibrium can not radiate in hard x-rays but instead produces a multi temperature black body spectrum peaking at $\lesssim 1 - 2keV$. So the hard x-rays seen from accretion events have to come from something other than an optically thick disc, perhaps from flares above the disc, or hot inner flow. We need to differentiate which geometry is present in the accretion flow around stellar mass black holes.

The aim of this thesis is to show that as the different geometries place the hard x-ray sources in different places, the x-ray spectra should be different. The x-ray images available do not have the spatial resolution necessary to determine the position of the source directly Nevertheless, as the relative position with respect to the cool thin disc is not the same, we believe we can differentiate the geometries through x-ray reflection.

Reflection

Some x-rays from the hot source will illuminate the cool disc. The disc can reflect some of the x-rays, imprinting on them some typical signatures not present in the illuminating spectrum (fig. 3.1). We now analyze the processes that can lead to a reflected spectrum.

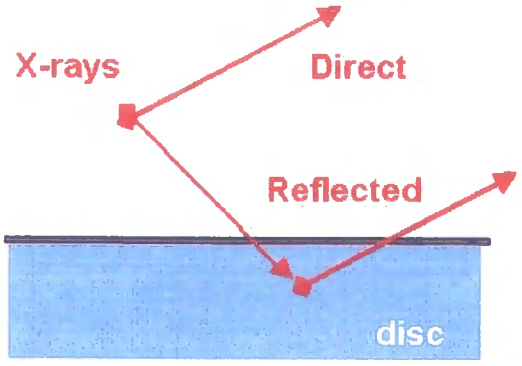

Figure 3.1: Schematic process of reflection by an accretion disc.

3.1 Neutral Reflection

We will start by considering reflection from a cool disc, in a neutral state of ionization, below a hot plasma source of hard x-rays. We assume a power law illuminating spectrum (see fig 2.2 in previous chapter), produced from multiple Compton scattering of some seed distribution of photons (generally a multicolour disc black body).

The illuminating x-rays can interact with the electrons in the disc by two principal mechanisms: photoelectric absorption, and Compton scattering. In order to reflect, the photons must Compton scatter and not be absorbed.

Photoelectric Absorption:

Electrons are bound to nucleons in atoms by electrostatic forces. When a photon with sufficient energy interacts with an electron it can ionize it. This will result in the photon losing its energy i.e. being absorbed.

Since the heavier elements have more protons in its nucleus, then their inner electrons are more tightly bound, so require more energy to be removed. Since iron is the highest atomic number element with appreciable abundance, it gives the highest absorption energies. For neutral material the photoelectric absoption edge for iron is at $7.1keV$. At lower energies there is much more photoelectric absorption as there are many low atomic number elements (C, N, O, Si, S,...), which can absorb $0.1 - 2keV$ photons. Since absoption is more important, reflection is less likely. Thus the amount of refelection rises sharply with energy from 0.1 to 10 keV (fig. 3.2).

The hole resulting from the electron ejection is filled by an electron from other orbital producing a fluorescence line or leading to the ejection of an outer electron (Auger effect). For lower atomic numbers Auger dominates over fluorescence emission, while the opposite is true for higher Z. Hence, the reflected spectrum has fluorescence lines from the heavier

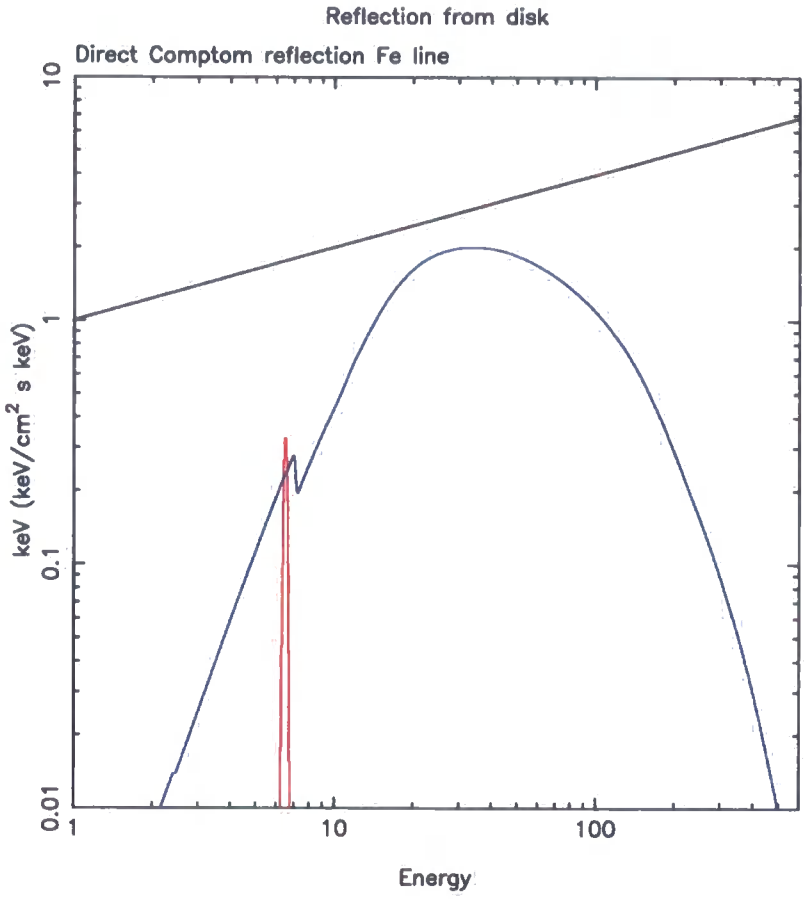

Figure 3.2: The illuminating power law and the reflection from a neutral disc, showing the broad peak and the iron edge. The iron emission line also appears but as an added component (in red).

elements, predominantly the Fe K line at $6.4keV$.

Compton Downscattering:

The encounter between photons and electrons can also lead to a different process, Compton scattering as described in section 2.1. When the energy of both the electrons in the disc and illuminating photon is low, then is very little energy exchange. The photon can be reflected back out to the observer at more or less the same energy as it came with. However, for high x-ray photon energies (close to $m_e c^2$), the photon can lose a substantial portion of its energy to the electron in the disc, in this case it is reflected with a much smaller energy that it originally had. This Compton Downscattering leads to a sharp rollover in the reflected spectra at high energies (fig. 3.2).

The overall effect is a balance between the two processes, Compton scattering and absorption. The low energy photons are absorbed, so few are reflected, and the iron line and edge

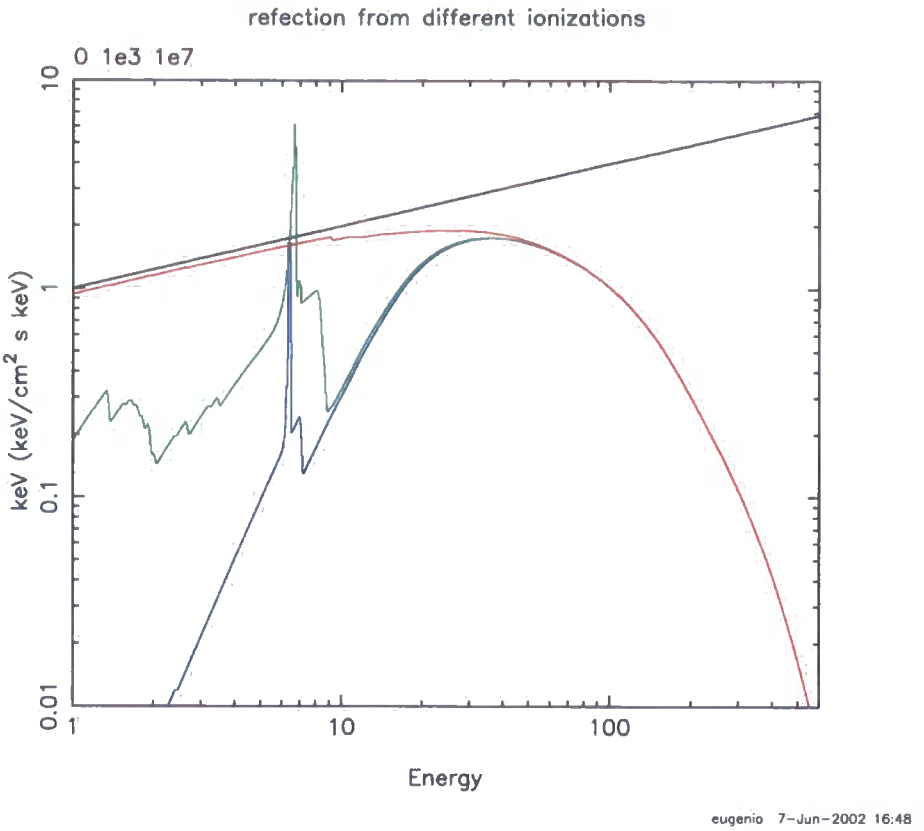

Figure 3.3: Reflected spectrum for three different ionization states: almost neutral state $\xi = 0$ (blue), ionized state $\xi = 10^3$ (green), and extreme ionized state $\xi = 10^7$ (red).

features are visible in the reflected spectra. At higher energies the reflected photons are downscattered to lower energies, rather than having the same energy as the illuminating photons. This all results in a spectrum which has a broad peak between $10 - 100keV$ (fig. 3.2).

Ionized Reflection

When the cool disc around the compact object is in an ionized (or partially ionized) state most of the atoms have none or very few electrons, so the photoelectric absorption is not that effective. Any remaining electrons are very tightly bound, so the edges and lines move to higher energies. For iron, which is the most important element in terms of observable diagnostics, the energies change to 6.7 and 8.8 keV for the line and edge for helium like iron, and to 6.95 and 9.3 keV for H-like iron.

The importance of photoionization can be estimated through the ionization parameter $\xi = L_x/n\mathbf{r}^2$, where L_x is the x-ray luminosity, n is the number density of ions and $\mathbf{r}$ is the distance to the x-ray source.

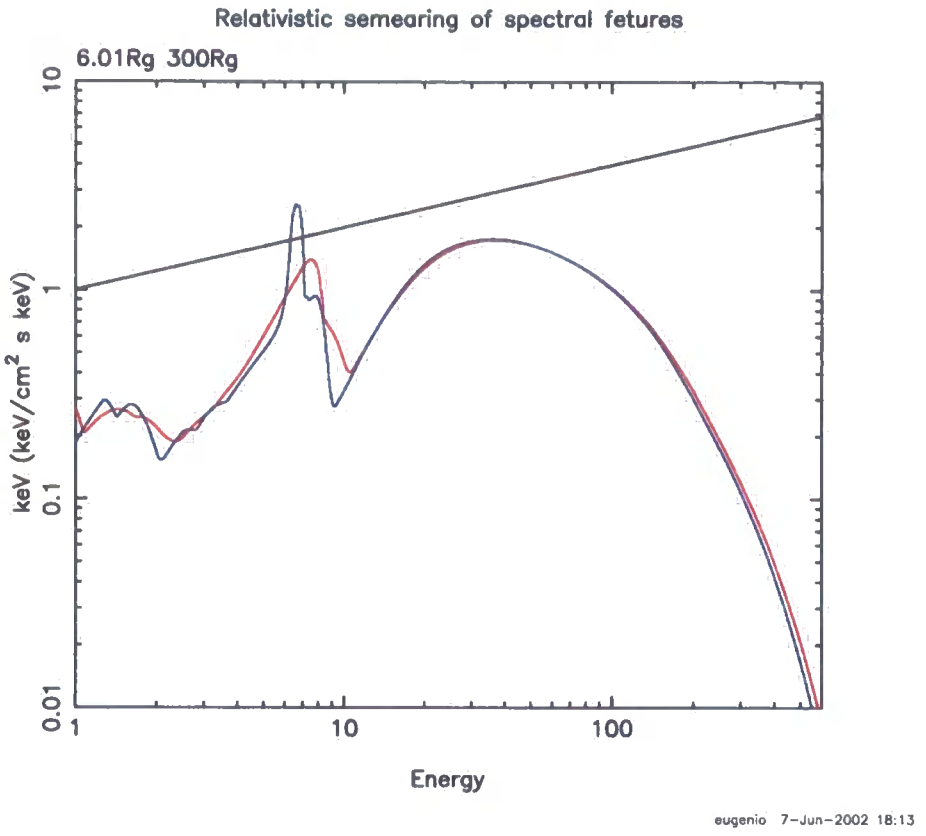

Figure 3.4: Relativistic effects with different strength related to different values of the inner radius ($R_{in} = 6R_g$ in blue and $R_{in} = 300R_g$ in red), assuming the same covering fraction.

Compton scattering is still effective, the less efficient photoelectric absorption gives a larger amount of reflection below 10 keV. When an extreme ionization state is reached, (i.e. when most of the electrons are stripped of their atoms), no photoelectric absorption or fluorescence emission is possible. So the reflection from a totally ionized disc will be dominated by Compton scattering, and it will be very similar to the direct emission below $10keV$ (fig. 3.3).

Relativistic Effects

The standard SS solution for the accretion disc allows it to have stable orbits down to six gravitational radii, defined as $R_g = \frac{R_s}{2} = \frac{GM}{c^2}$, where M is the mass of the central object.

Coming from so deep in the potential well it is expected that the emission from the disc will be affected by the strong gravity. This effect is expected to be more easily observed in the smearing of the iron line (because the Fe K line is the strongest narrow feature). The smearing of the iron line is due to a combination of four effects: aberration of light,

transverse redshift, doppler shift, and gravitational redshift (Fabian et al. 1989).

The doppler effect will redshift the emission line (and reflected continuum) from the side of the accretion disc that is receding from us, and blueshift the one approaching. This leads to a broadening of the line around the value for emission (at a given ionization state). This amount of broadening, together with companion eclipses, may also help to constrain the inclination of the system.

The two remaining special relativistic effects are due to the high speed of the material in the inner orbits. Aberration of light will lead to a beaming of the blue part, as emission from high speed emitters is anisotropic, favoring the direction of motion. Conversely, the red side is suppressed, leading to a skewed line profile. The second effect is the redshift of the line as time dilates for the emitters at velocities approaching that of light.

Finally gravitational redshift will redshift the whole line as radiation loses energy as it climbs up the gravitational potential well.

It is worthy noting that the strength of the observed effect depends on the geometry, as the special and general relativistic effects are negligible if the disc does not extend to the last stable orbit but truncates at a much larger distance from the source. Fig. 3.4 shows the predicted spectra for a neutral disc with different values of the most inner orbit.

3.2 Reflection & Geometry

The two main potential geometries for accretion flows are known as truncated disc model and magnetic flares model. The physical mechanisms supporting this models were outlined in section 2.2, and here the observational predictions of each model will be discussed, mainly in terms of its reflection signature, as this is crucial for understanding the true geometry.

As the physical processes governing the reflection are the same for both models, we have to rely on the geometry for their differentiation. The main geometrical difference between the models is the relative position of the disc and the hot plasma. For the magnetic flares models, the hot electrons are above the disc, while for the truncated disc model they fill a hole in the centre of the disc. This difference in geomerty leads to a difference in the covering fraction parameter, $\Omega/2\pi$, of the disc as seen from the x-ray source. In the magnetic flares model the disc covers half of the sky, while in the truncated disc model only 30% or less is covered. This leads to different *amount* of reflection expected from each geometry.

Assuming a neutral or intermediate level of ionization, the truncated disk model predicts a smaller reflected component, so the overall spectrum will have the reflected fea-

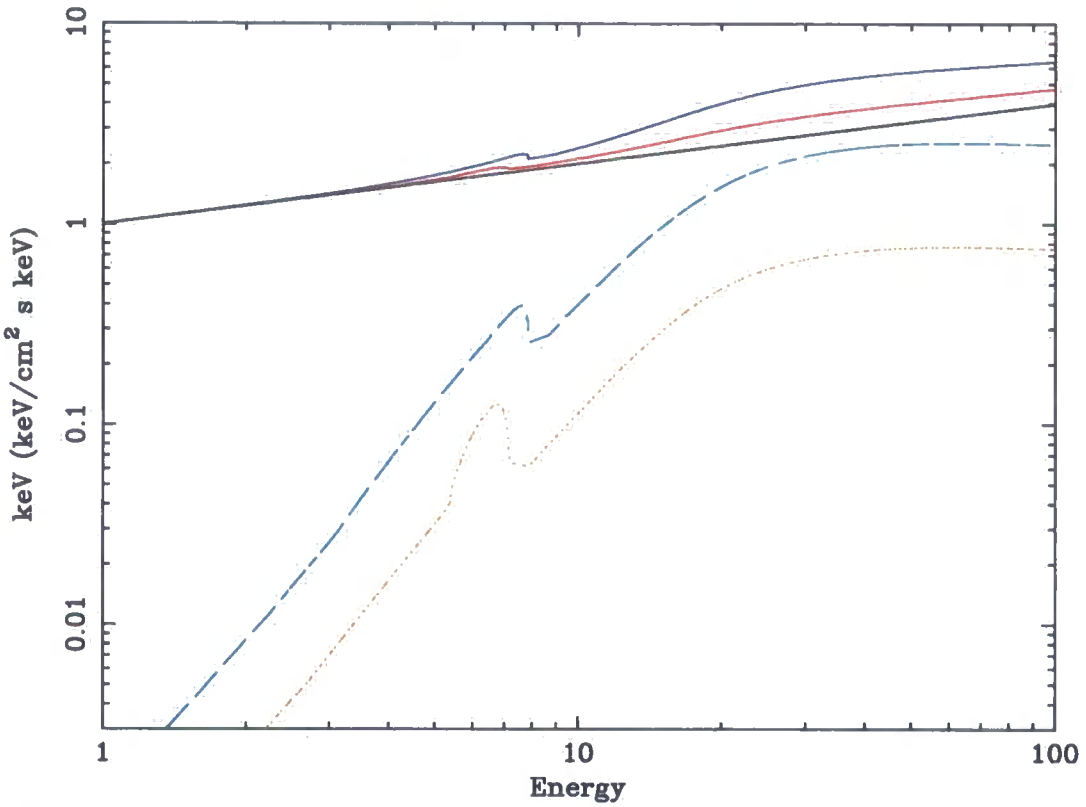

Figure 3.5: The illuminating power law over a neutral disc is shown in black. The magnetic flare model is the red set while the truncated disc model is in blue. The full lines are the total spectrum prediction while dashed lines are the reflection components. Note the much stronger reflection and broader iron line/edge features from the untruncated disc magnetic flares model in comparison to the truncated disc reflection.

tures (absorption, lines, etc.) diluted by the continuum. Conversely in the magnetic flares model, there is a stronger reflected component, so the spectra shows a larger iron line and deeper edge.

Moreover, as seen from the previous section, the amount of smearing in the Fe line will tell us how far the thin disc extends into the potential well. So for the truncated disc geometry the smearing should be negligible, while for the magnetic flares models it should be strong (fig. 3.5).

3.3 Previous Observations

The black hole binaries spectra in the low/hard state show overwhelmingly that the solid angle subtended by the disc from the x-ray source is significantly less than 2π, and that the smearing of the iron line is less than expected for a disc extending down to the last stable orbit (Życki Done & Smith 1997; 1998; 1999; Gierliński et al. 1997; Done & Życki 1999; Zdziarski et al. 1999; Gilfanov, Churazov & Revnivtsev 1999; 2000). While this is clearly consistent with the idea that the disc is truncated in the low/hard state, the magnetic flare models can be retrieved in several ways.

Firstly, magnetic reconnection on the Sun is known to produce an outflow, the coronal mass ejection events. In the extreme conditions close to the black hole it is possible that this outflow velocity could be large so that the hard x-ray radiation is beamed away from the inner disc (Beloborodov 1999).

An alternative explanation for the lack of reflection and smearing is that the inner disc or top layer of the inner disc is completely ionized. There are then no atomic features, and the disc reflection is unobservable in the 2–20 keV range as it appears instead to be part of the power law continuum (Ross & Fabian 1993; Ross, Fabian & Young 1999). However, these models with passive illumination of the disc require a fairly sharp (vertical or radial) transition between the extreme ionization and mainly neutral material (Done & Życki 1999; Done, Madejski & Życki 2000; Young et al. 2001). A sharp vertical transition can be produced as the disc *responds* to the intense X–ray illumination. There is a thermal ionization instability which affects X–ray illuminated material in pressure balance, which can lead to a hot, extremely ionized skin forming on top of the rest of the cooler, denser, mainly neutral disc material (Field 1965; Krolik, McKee & Tarter 1981; Kallman & White 1989; Ko & Kallman 1994; Różańska & Czerny 1996; Nayakshin, Kazanas & Kallman 2000, hereafter NKK; Różańska & Czerny 2000; Nayakshin & Kallman 2001; Ballantyne, Ross & Fabian 2001).

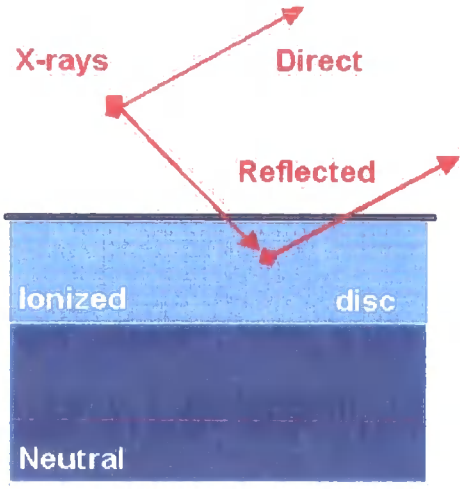

Figure 3.6: Schematic reflection from a disc and ionization instability

Thermal Ionization Disc Instability

When a strong illumination acts over a disc in hydrostatic equilibrium, the surface temperature depends on the trade off between the heating and cooling processes.

The typical Compton temperature for a disc illuminated with a hard x-ray spectrum ($\Gamma \sim 1.7$), can be as high as $10keV$. At this temperature the top of the disc is completely ionized. As we move inside the disc, the temperature drops as some of the illuminating flux is shaded by the top layer. However the pressure must increase as the disc is in hydrostatic equilibrium. Since $P_{gas} = nkT$, the only way for the pressure to rise as the temperature drops is for the density to rise. Bremsstrahlung cooling then becomes more important, as it depends on n^2. This additional cooling brings the temperature down even more quickly. The net result is that temperature drops dramatically with a small increase in depth. When temperature reaches $1keV$, line emission becomes important, helping the cooling even more. So the material makes a rapid transition to a cool layer (fig. 3.6). The depth at which this occurs is determined by the balance of the luminosity from the x-rays and the luminosity from the disc L_x/L_d.

This extreme ionization skin over a cooler, more neutral material can produce a spectrum that has no iron features, i.e. has a reflected spectrum that looks like direct emission below $10keV$. Estimates of the covering fraction based on the observed strengh of the iron line/edge features, can be wrong if this effect is not taken into account (Done & Nayakshin 2001a).

The ionization instability is only significantly present in the magnetic flares models as the ξ parameter has to be high (due to strong L_x, small distance and low density). In the truncated disc models the typical distance of the x-ray source is much further from

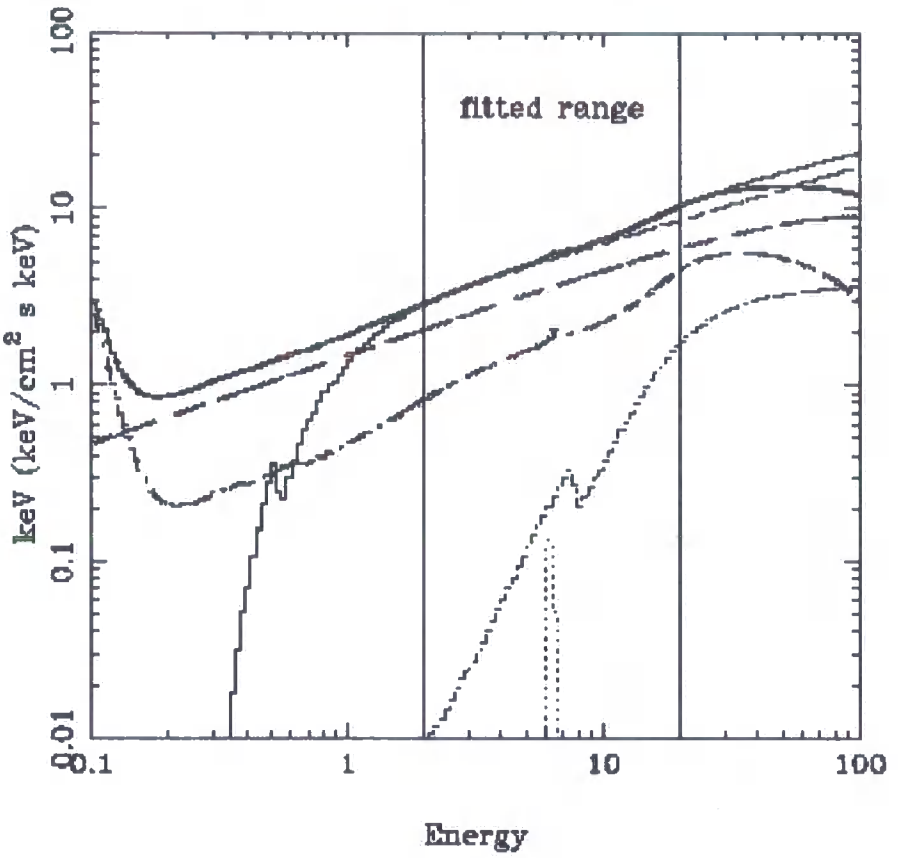

Figure 3.7: Model spectra from truncated disc (thin lines) and magnetic flares (thick lines) geometries. The overall spectra in the $2-20keV$ range can be identical, although the model components are very different. The truncated disc has strong intrinsic continuum (dashed-dot line) and weak neutral reflection (dashed line), while the magnetic flares have weaker continuum and much more reflection (Done & Nayakshin 2001a).

the disc, so L_x/L_d is much lower and the ionized skin is very shallow and makes little difference to the reflected spectra.

The predicted spectra of both models can then be very similar. The magnetic flare model over an untruncated disc with ionized skin, can give the same weak observed reflection as predicted from a truncated disc models (fig. 3.7) (Done & Nayakshin 2001b).

3.4 Testing the Geometry

While the truncated disc and magnetic flare/x-ray illuminated disc models are indistinguishable with current data in the $2-20keV$ range, they are very different at higher

energies. In the magnetic flare models, a lot of the $2-10keV$ continuum is actually ionized reflection, so the true continuum level is lower than in the truncated disc models, in which reflection is small. At higher energies, where reflection is negligible, the lower continuum level for the magnetic flare models leads to a smaller predicted flux in the $100-200keV$ range than for the truncated discs (Done & Nayakshin 2001a) fig 3.7 (high energies). In the next chapter both truncated disc and magnetic flare/x-ray illuminated disc models are fitted to the $3-200keV$ PCA/HEXTE spectrum of the hard/low state spectra of Cyg X-1. We show that the truncated disc models provide an excellent fit to these data, but that the magnetic flare/x-ray illuminated disc does not, as it dramatically under–predicts the $100-200keV$ spectrum.

Chapter 4

Modeling

Astronomy compels the soul to look upwards
and leads us from this world to another.

Plato

As shown in the previous chapter, the different geometries predict spectra that are very similar in the typical range $(2 - 20keV)$ where we have data. However, they are different if we move to higher energies (e.g. $50 - 200keV$). Spotting whether direct emission or reflection is the dominant component in this range, will tell what geometry is present in the hard state of the accretion discs around black holes.

4.1 The Instrument

In order to determine the geometry, we need data from an accretion flow around a black hole, in the form of its x-ray spectra in a very broad band ($\sim 2 - 200keV$). This spectrum can not be obtained by the same instrument, because most of the instruments are designed and optimized for narrower bandwidths. But a combination of instruments will be able to support the required broad spectrum. The only current detectors in this range are PCA and HEXTE, both instruments on board RXTE.

The Rossi X-ray Timing Explorer RXTE was launched on December 30, 1995 from NASA's Kennedy Space Center. The mission is managed and controlled by NASA's Goddard Space Flight Center (GSFC) in Greenbelt, Maryland. RXTE features unprecedented time resolution in combination with moderate spectral resolution to explore the variability of x-ray sources. Time-scales from microseconds to months are covered in an instantaneous spectral range from 2 to 250 keV. Originally designed for a required lifetime of two years with a goal of five, RXTE has passed that goal and is still performing well.

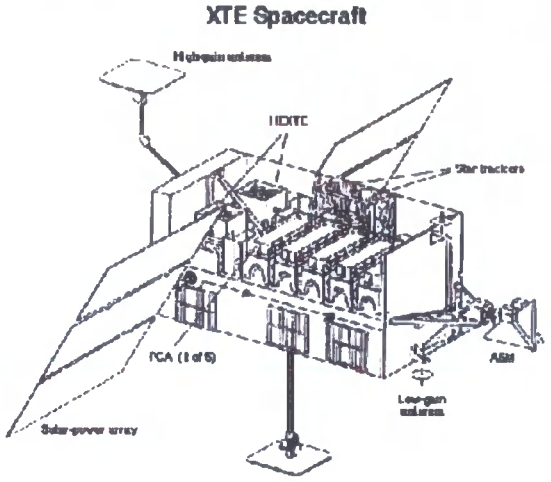

Figure 4.1: Diagram of RXTE satellite showing main parts and instruments. NASA GSFC RXTE webpage.

The mission carries two pointed instruments, the Proportional Counter Array (PCA) developed by GSFC to cover the lower part of the energy range ($2 - 60keV$), and the High Energy X-ray Timing Experiment (HEXTE) developed by UCSD covering the upper energy range ($15 - 250keV$). These instruments are equipped with collimators yielding a full width at half maximum of one degree (fig. 4.1)[1].

X-ray detectors, in general, have a very complex non Gaussian response. In order to analyze the data we need to deconvolve the intrinsic spectrum from the effects of this instrument response, regrettably this is not possible in general, as such inversions tend to be non-unique and unstable to small changes in the photon counts (Arnaud, et al. 1992).

Instead, we work with models (see next section) designed to be used with XSPEC (Arnaud, 1996). XSPEC is a command-driven, interactive, x-ray spectral-fitting program. It is designed to be completely detector-independent so that it can be used for any instrument.

XSPEC takes as input data files, background and instrument responses from the satellites. The program creates a synthetic model spectra in the same fashion, convolving the instrument response with the model. Then this covolved model spectra is compared with the data. The model parameters are varied to find the parameters values that give the best fit statistic. The fit statistic used is χ^2.

[1]This information can be found in RXTE webpage, Goddard Space Flight Center, NASA: http://heasarc.gsfc.nasa.gov/docs/xte/XTE.html

4.2 The Models

The model spectra should incorporate all the physical processes happening in and around the accretion discs. The total spectrum is built up from several independent model components, where each one focuses on representing a particular characteristic of the system. Some of them produce the disk emission, others, the iron line, others a complex ionized reflection, etc.

Continuum Models

The simplest approximation of the continuum emission from the hot region in accreting events is a power law plus and exponential cutoff. The typical values for hard x-rays spectral indexes are $\Gamma = 1.7 - 1.9$, while the cutoff energy is at about $100 - 150keV$. This is the first approximation for the multiple Compton upscattering (see fig. 2.2) of a much cooler emission from the disc, the cutoff energy constrains the temperature of the hot plasma. Although it is a common approximation it is not very accurate. By contrast COMPPS (Poutanen & Svensson 1996) calculates the Compton scattering very carefully, allowing different geometries for the hot region, and even anisotropic illumination from the disc. It includes spherical and half spherical symmetries, slab and cylinder. It also has a 'flag' that allows for reflection (fig. 4.2) from the disc, but this has very crude ionization balance and does not include any vertical structure (Done et al. 1992).

Reflection Models

The XPEC package comes with the standard PEXRIV of Magdziarz & Zdziarski (1995) (fig. 3.2). This is the reflection code used by COMPPS, so again it employs an aproximate ionization balance and neglects vertical structure of the disc (Done et al 1992).

We use instead, the complex ionization reflection code XION, described in Nayakshin, Kazanas & Kallman (2000), which computes the self-consistent vertical ionization structure of an x-ray illuminated disc in hydrostatic equilibrium at a given radius. The reflected and diffuse (line and recombination continua) emission from this are smeared by the relativistic effects expected from a disc, and then these spectra are summed over all radii to get the total disc reflected emission for any given source/disc geometry. These models have been tabulated for a central sphere/truncated disc geometry, assuming that the hot inner flow has emissivity $\propto r^{-3}$, and starts at the radius where the optically thick disc truncates (Nayakshin et al. 2002, in preparation). Models have also been tabulated for a magnetic flare geometry, which results in much stronger illumination of the disc and so gives a deeper ionized skin (Nayakshin 2000). With magnetic flares, the luminosity of the

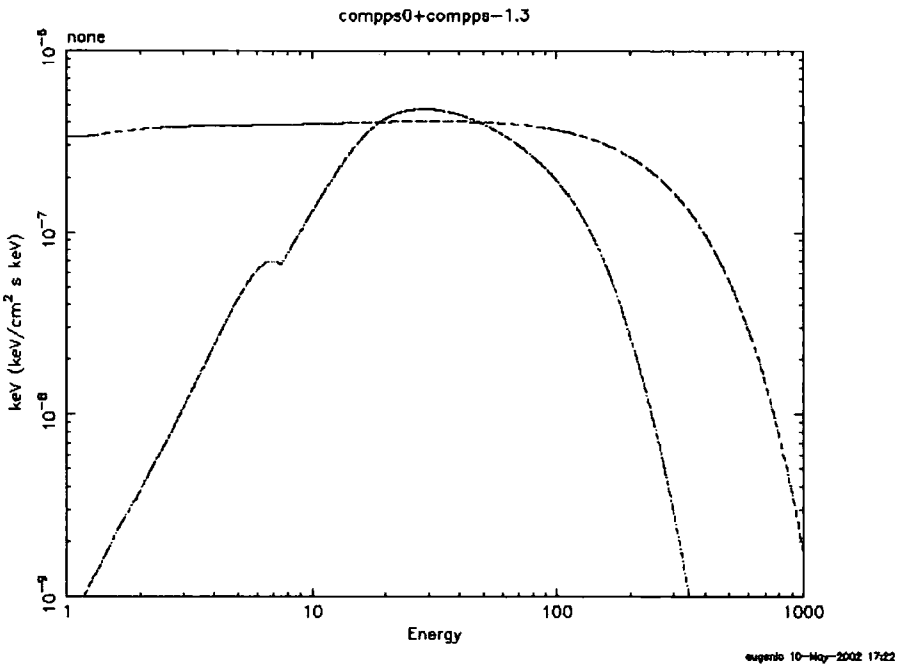

Figure 4.2: COMPPS model of direct emission for a sphere; and COMPPS direct plus reflection with a covering fraction of 0.3.

flares is assumed to scale as the local disc flux, so that f_x/f_{disc} remains constant with radius.

A comparison of XION and PEXRIV reflection

The main objective of the XION code is to accurately calculate the vertical ionization structure of the x-ray illuminated disc, so the atomic physics/photoionization calculations are treated in great depth while Compton scattering is approximated in the same manner as in Ross & Fabian (1993). These approximations are adequate at lower energies, where the energy shifts from Compton scattering are small, but become progressively less accurate at higher energies where downscattering is large. By contrast, the standard PEXRIV reflection model in XSPEC treats Compton scattering very carefully (Magdziarz & Zdziarski 1995), but has very crude ionization balance and does not include any vertical structure (Done et al. 1992).

The two codes should give comparable results when the vertical structure is unimportant i.e. when the x-ray illumination is very small. Fig. 4.3 shows a comparison of the two codes, the solid red line describes the results from the lowest illumination possible in the tabulated XION models ($f_x/f_d = 0.02$ and $\dot{M} = 0.001$) for a magnetic flare geometry

at inclination angle of 30°. The dotted blue line shows the comparable PEXRIV results ($\Omega/2\pi = 1$, $\xi = 0$, inclination of 30°). The continuum for both is an illuminating power law of index $\Gamma = 1.7$ with exponential rollover at $300keV$. The differences are obvious. At low energies these are expected as the XION code has a residual ionized skin in even a weakly illuminated disc. One would have to extend the grid in XION to even lower values to render effects of the skin completely negligible in the soft x-ray range. The ionization effects should nevertheless be very small at high energies where the two codes should yield very similar results. However the Compton hump extends to much higher energies in PEXRIV than in XION, and the normalization is different by a factor of 1.3 at 20 keV.

The difference in normalization is due mainly to the difference in illumination law used. Magdziarz & Zdziarski (1995) have specific intensity $\propto 1/\cos\theta$, while XION assumes a single ray, incident onto the surface at 45°. The first form of the illumination law is appropriate for an optically thin *full* corona (with a covering fraction equal to unity) which is now known not to work for Cyg X-1 (Gierlinski et al. 1997); the use of a fixed value of $\theta = 45°$ in XION, on the other hand, stems from the necessity to keep the XION runtime to a manageable minimum. Thus both illumination laws are not expected to be strictly correct in reality and are approximations good to some 10-20 %.

The deficit of photons at $\sim$ 200 keV is a more serious problem. It is mainly due to the energy grid of XION only extending to $200keV$, again from the need to keep the XION runtime to a manageable level. However, it is these high energy continuum photons (which are included in PEXRIV) which are downscattered to form the reflected continuum above $30keV$. Thus XION as tabulated here gives too few reflected photons at high energies compared with PEXRIV.

An ideal model would accurately calculate *both* the ionization structure and Compton scattering for a broad range of parameters and do it *fast*. Since such model is not feasible due to computer limitations, we use the ionization structure of XION at low energies ($< 20keV$) and the Compton downscattering calculations of PEXRIV at high energies (> 30 keV), having matched the normalization of the PEXRIV reflection to that of XION at $20keV$. The gap in good data between $20 - 30keV$ means that the two different models can be used for the PCA and HEXTE data, respectively, rather than having to interpolate between them.

We have called our models after the geometry they represent so we have: XION-DISC and XION-FLARES. The free parameters are the mass accretion rate (this determines the unilluminated disc structure i.e. the starting density as a function of height), f_x/f_{disc}

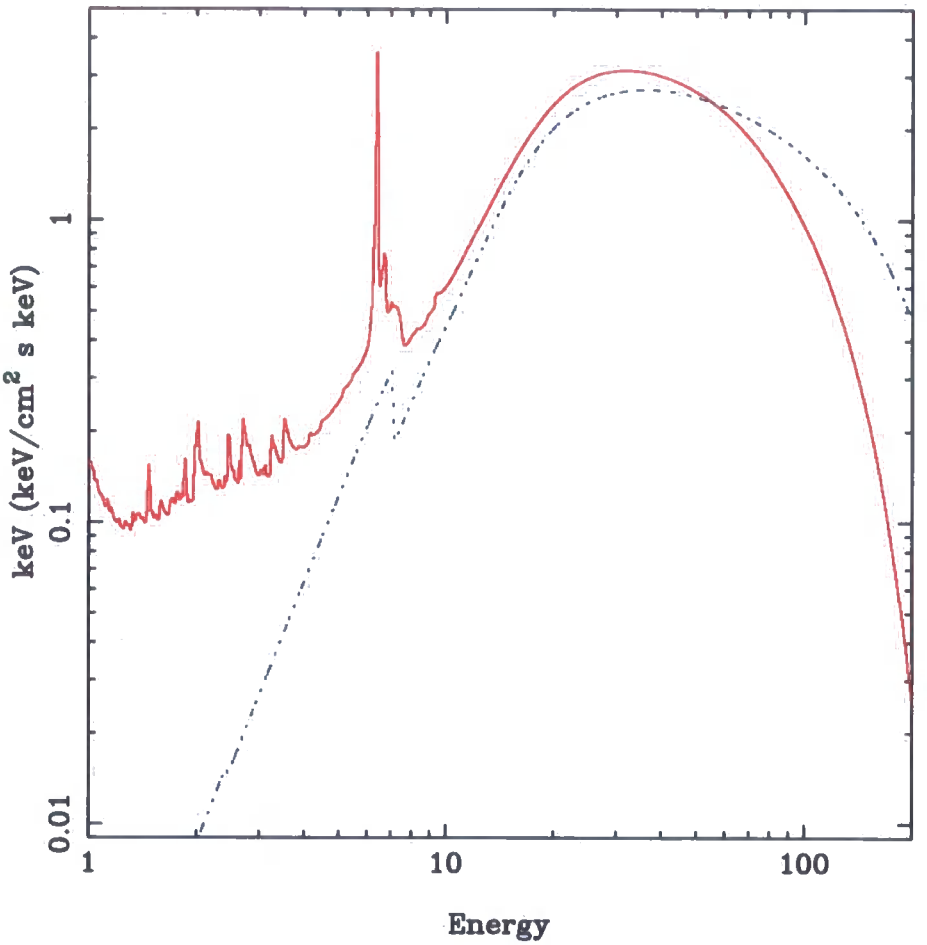

Figure 4.3: The solid line shows the lowest ionization XION reflected spectrum from a power law continuum with $\Gamma = 1.7$, with exponential rollover at 300 keV. We use the XION-FLARE model, so the disc subtends a solid angle of 2π, and assume an inclination of 30°. The dashed-dotted line shows the reflected spectrum calculated under the same conditions using the PEXRIV model. xion-flare predicts much more reflected flux at low energies as even at the lowest tabulated ionization there is still a residual, low optical depth, ionized skin which reflects a small fraction of the continuum. The difference in shape at high energies and the slight difference in normalization at 20-30 keV is due to the approximate treatment of Compton downscattering in the XION code and the different assumed illumination.

which determines the depth of the ionized skin, and the shape of the illuminating spectrum (Γ and E_{cut} assuming an exponentially cutoff power law). For the truncated disc models there is also the inner radius of the accretion disc, R_{in}, which controls the amount of relativistic smearing of the iron line features.

4.3 The Spectra

We choose Cyg X-1 as our source for the following reasons. Cyg X-1 has been known since 1970 as a powerful x-ray source. Nowadays it is widely known as a prototypical and best studied black hole binary. It is a high mass x-ray binary the optical counterpart is a supergiant O9.7IaS HD26868 (Webster & Murdin, 1972), Bolton, 1972)of about $30M_{\odot}$. The orbital period is $P = 5.6days$, amplitude of $K = 75Km/s$, the inclination of the system $i \sim 30°$. The mass of the black hole is estimated between 10 and 16 $M_{\odot}$ (Kubota 1998, Liang & Nolan 1983), and the distance is $2kpc$ (Gierlinski et al. 1999).

The spectra of Cyg X-1 also show the hard to soft variably mentioned before (chapter 2). In the hard state the spectra exhibits a single power law shape with an exponential cut off near 100 keV. In contrast, its soft state is characterized by a dominant soft emission below $10keV$, accompanied by a hard power law tail extending to $500keV$ and beyond (Gierlinski et al. 1999).

We used the hardest spectra seen from multiple observations of the Cyg X-1 hard/low state (Gilfanov et al. 1999). We extracted the data using the REX data analysis script with the bright source background from the top layer of PCA detectors 0 and 1. Previous work has shown that this configuration gives a good fit to the Crab data with 0.5 per cent systematic error for RXTE Epoch 3 data (Wilson & Done 2001). We extracted the simultaneous HEXTE data from cluster 0. In fits with both the PCA and HEXTE data we allow a normalization offset between the two instruments to take into account the cross-calibration uncertainties. We use XSPEC version 11 (Arnaud et al. 1996) and quote all error bars as $\Delta\chi^2 = 2.7$, corresponding to 90% confidence limits on 1 parameter.

First Analysis

First we fit with naively simple models to corroborate the sensible values of the fixed parameters like the hardness of the power law $\Gamma = 1.7$ (Gilfanov et al. 1999), the absorbing column of $N_H = 6 \times 10^{21}$ cm^{-2} (Bałucińska-Church et al. 1995), the mass accretion rate $\dot{M} = 0.03$, etc.

Then we fit the PCA data alone with the old, single ionization parameter reflection models so that we can compare the new reflection models with previous fits (fig. 4.4).

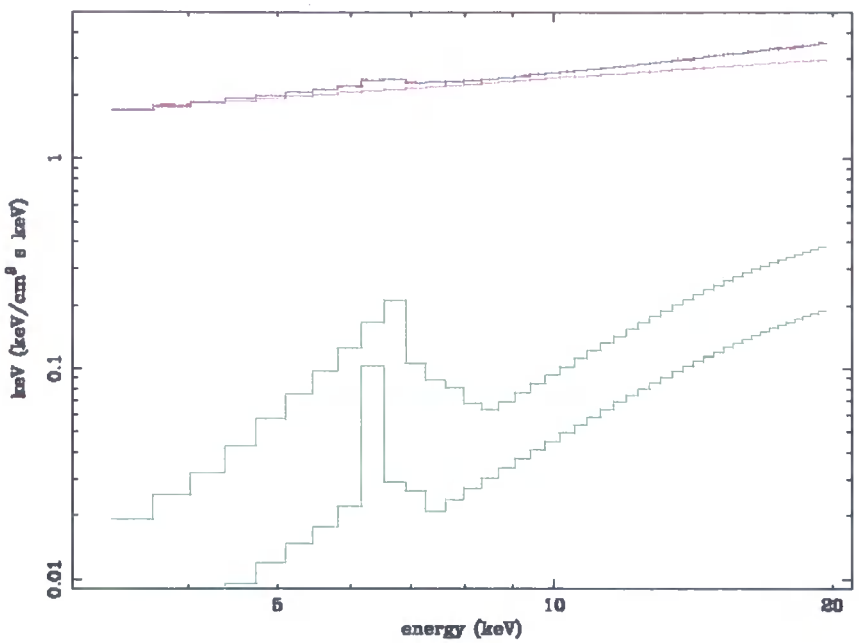

Figure 4.4: Cyg X-1 PCA data fitted with a single ionization model. Data in red, illuminating continuum in magenta, the reflected component by the disc and by a companion star in green, while the total spectrum is in blue.

We use the REL-REPR model of Życki et al. (1998), which is based on the publically available PEXRIV reflection but includes the self consistently produced iron line emission and relativistic smearing. We assume a power law continuum model, and also include neutral, unsmeared reflection which can arise from the companion star or outer accretion disc (Ebisawa et al 1996). This gives a $\chi^2_\nu = 30/39$ and the amount of reflection from the accretion disc is low, with $\Omega/2\pi = 0.13 \pm 0.08$, naively implying a truncated disc.

We then replace the single ionization accretion disc reflection with the XION-DISC model. The simplest version of this truncated disc geometry assumes the hot inner source is spherical, and starts where the cool disc truncates. This results in a model in which $\Omega/2\pi$ is fixed at ~ 0.3, rather larger than inferred from the simple reflection models above, and so gives a somewhat larger $\chi^2_\nu = 53/40$. If instead we allow the amount of reflection to be smaller than this (e.g. if the hot source has a flattened rather than spherical geometry) then we get $\chi^2_\nu = 43/39$ for $f_x/f_d = 6$. This is a worse fit by χ^2 of 13 than that for the single ionization zone reflection models (REL-REPR, above). The two models give different fits as even a weakly illuminated disc produces a low optical depth ionized skin (see fig. 4.3). This reflects some small fraction of the incident continuum at low energies

We use XION-FLARE to model the magnetic flare geometry in which $\Omega/2\pi$ is fixed at 1 and the inner disc extends down to three Schwarzschild radii. This gives $\chi^2_\nu = 47/41$

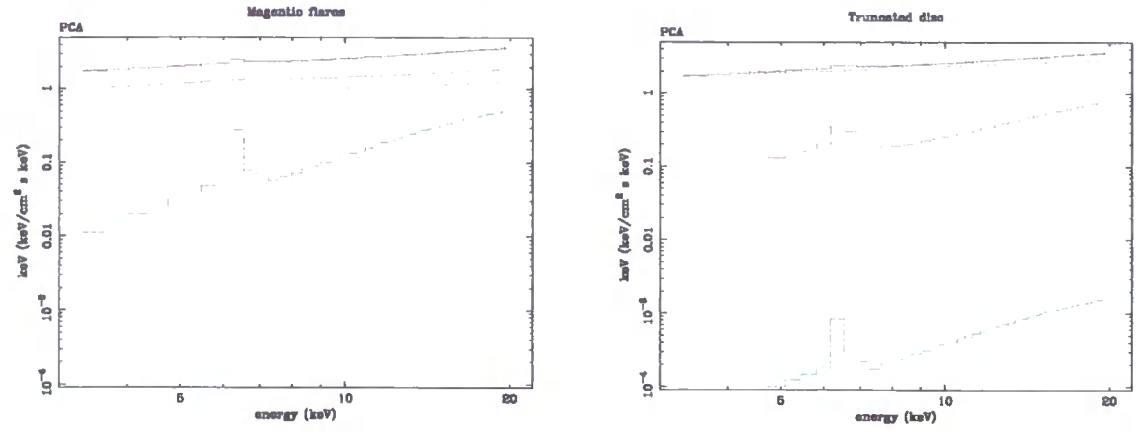

Figure 4.5: Fit with truncated disc and magnetic flares models to Cyg X-1 PCA data ($3-20keV$). Data is in red, total model spectrum in blue: the doted orange is the illuminating continuum, the dashed magenta the disc reflection the dot dashed light blue reflection from companion star.

(both the solid angle of reflection and the inner disc radius are fixed, leading to two fewer degrees of freedom). This confirms the results of Done & Nayakshin (2001b) that magnetic flares can give as good a fit to the data below $20keV$ as a truncated disc. The PCA data are consistent with the presence of a large amount of ionized reflection, i.e. with a disc which subtends a large solid angle to the x-ray source and extends down to the last stable orbit.

The fits are shown at the same scale in fig. 4.5 for comparison.

However, these two very different reflection models should give very different spectra at higher energies. Reflection *must* rollover at high energies due to Compton downscattering in the disc. Fig. 4.6 shows the truncated disc (upper panel) and magnetic flare (lower panel) PCA fits extrapolated to the HEXTE data. The truncated disc model has little reflection, so there is little rollover in the total spectrum. By contrast, the magnetic flare models have a lot of highly ionized reflection, so the contribution of the Compton downscattering rollover is important. Plainly there is no such rollover in the HEXTE data, and the magnetic flare description of the PCA data strongly underestimates the higher energy spectrum. This is made even more marked by the fact that a power law is an overestimate of the high energy continuum: a true Comptonized continuum has a thermal cutoff at $150-200keV$ (Gierliński et al. 1997). By contrast, the truncated disc models can qualitatively describe the high energy data.

While this argues strongly against a large ionized reflection component in the data, true spectral fitting is required to show conclusively that this is the case.

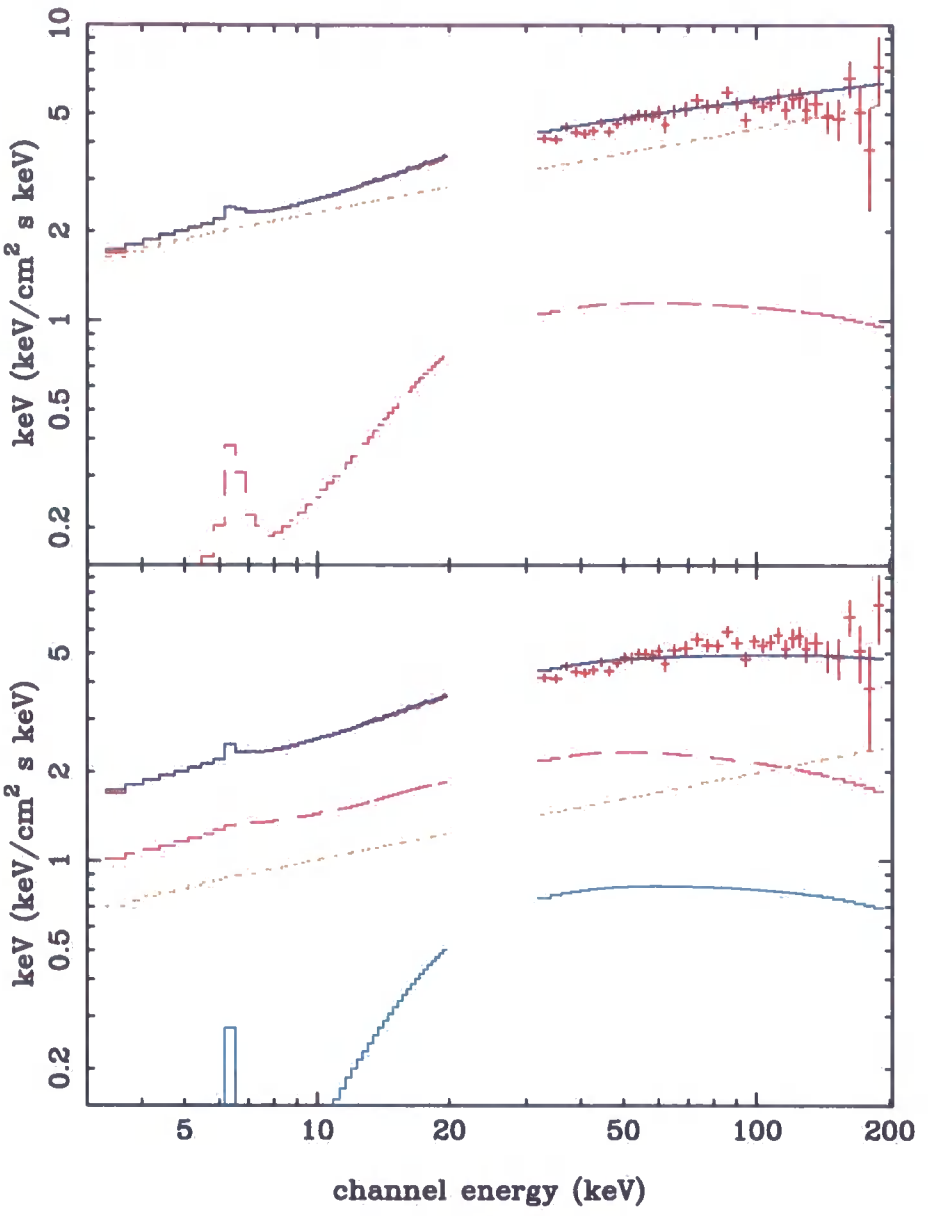

Figure 4.6: The upper panel shows the PCA fit to a power law and truncated disc model extrapolated through the HEXTE data, while the lower panel shows this for the magnetic flares. Both figures have the power law continuum as a dotted line, while the dashed line is the reflected component from the accretion disc. The intrinsic continuum level for the truncated disc is much higher than for magnetic flares as the magnetic flares have a large contribution of reflected emission in the PCA. The reflected continuum has a *rollover* at $\sim$ 100 keV, so the extrapolated high energy spectrum is dominated by the intrinsic continuum and the magnetic flare model predicts a much smaller HEXTE flux than the truncated disc. Both fits have comparable χ^2 in the PCA, but the magnetic flares underpredict the high energy data while the truncated disc model matches fairly well. Both fits include neutral, unsmeared reflection from the companion star/outer disc (lower solid line in the bottom panel) but is too small to be seen in the truncated disc model.

4.4 Fitting to High Energies

For a single temperature Compton continuum fit to the data above 10 keV in this approach with the XION-DISC model gives $\chi^2_\nu = 62/59$. By comparison, the reflection model built into the COMPPS code (which is based on PEXRIV) has $\chi^2_\nu = 65/59$ showing that the matching condition is adequate.

We do joint fits of the PCA and HEXTE data, using the Comptonization model, COMPPS, of Poutanen & Svensson (1996) rather than a power law for the continuum. In all the fits we also allow this also to illuminate the companion star, producing a neutral, unsmeared reflection component. The PCA and HEXTE flux give a luminosity of $\sim 10^{37}$ ergs s^{-1}, or $\sim 0.01 L_{\rm Edd}$. This is $\sim 3\times$ lower than the luminosity seen in a BeppoSAX observation, where the seed photon temperature was observed to be ~ 0.15 keV (di Salvo et al. 2001). Hence we fix the seed photons for Compton scattering at a temperature of $3^{-1/4} \times 0.15 = 0.1$ keV.

We first assume that the Comptonizing region is spherically symmetric, illuminated by isotropic seed photons to produce a generic, isotropic Comptonized continuum (geometry flag set to 0). This gives an adequate fit of $\chi^2_\nu = 114/77$ where this continuum is assumed to form a spherical central source which then illuminates a truncated disk (i.e. with hardwired solid angle of $\Omega/2\pi = 0.3$). Allowing the reflection amount to vary (as in a flattened source) gives a much better fit with $\chi^2_\nu = 86/76$. We show the unfolded spectrum and residuals from this model in fig. 4.7, where the continuum parameters are $\tau \sim 0.75$ and $kT_e = 200keV$. By contrast, assuming the isotropic continuum is above the disk, as appropriate for magnetic flares, gives a very poor fit, with $\chi^2_\nu = 259/78$ (fig. 4.8) for a continuum with $\tau \sim 0.75$ and $kT_e \sim 210keV$.

However, both these fits are subtly inconsistent as the continuum model assumed isotropic seed photons for the Compton scattering rather than having them arise from the disk. Anisotropic seed photons lead to anisotropic Compton continuum (e.g. Haardt & Maraschi 1993), so a fully self-consistent picture should include the continuum anisotropies which arise from the two different geometries. There is a fairly large range of incident angles for the seed photons in the truncated disc geometry so we expect any anisotropies to be small (so the isotropic continuum models above should be a good approximation), but the magnetic flares are illuminated preferentially from below. For a Comptonizing plasma with optical depth of order unity and temperature of ~ 200 keV (Sunyaev & Titarchuk 1980; Gierliński et al. 1997) then this seed photon anisotropy can have a marked effect on the spectrum (Haardt & Maraschi 1993; Poutanen & Svensson 1996). We use the COMPPS code to simulate the anisotropic continuum expected from hot plasma forming a slab above

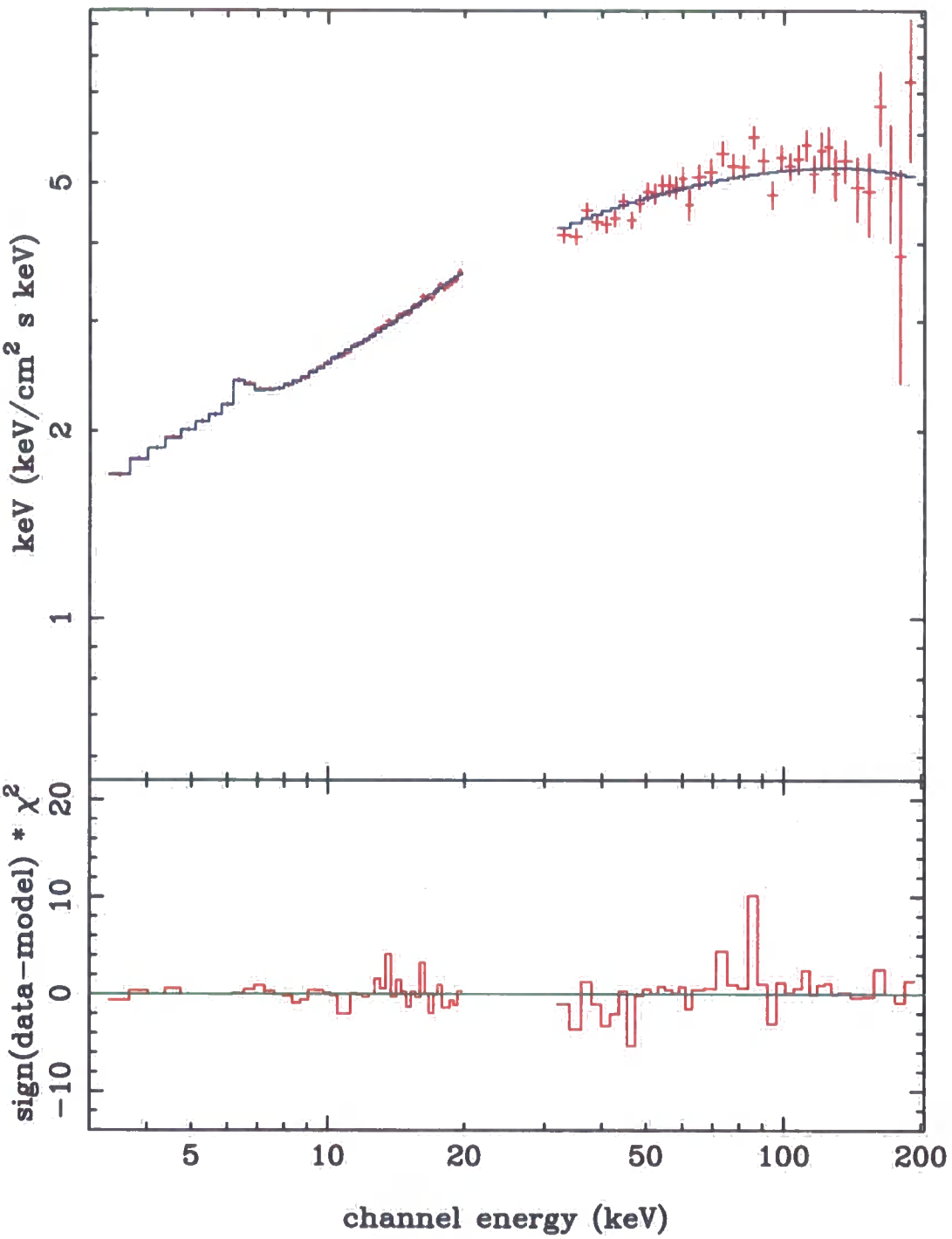

Figure 4.7: The PCA and HEXTE data fit to a Comptonized continuum plus illuminated truncated accretion disc model XION-DISC, plus neutral, unsmeared reflection from the companion star/outer disc. The upper panel shows the unfolded spectrum while the lower panel shows residuals to the fit.

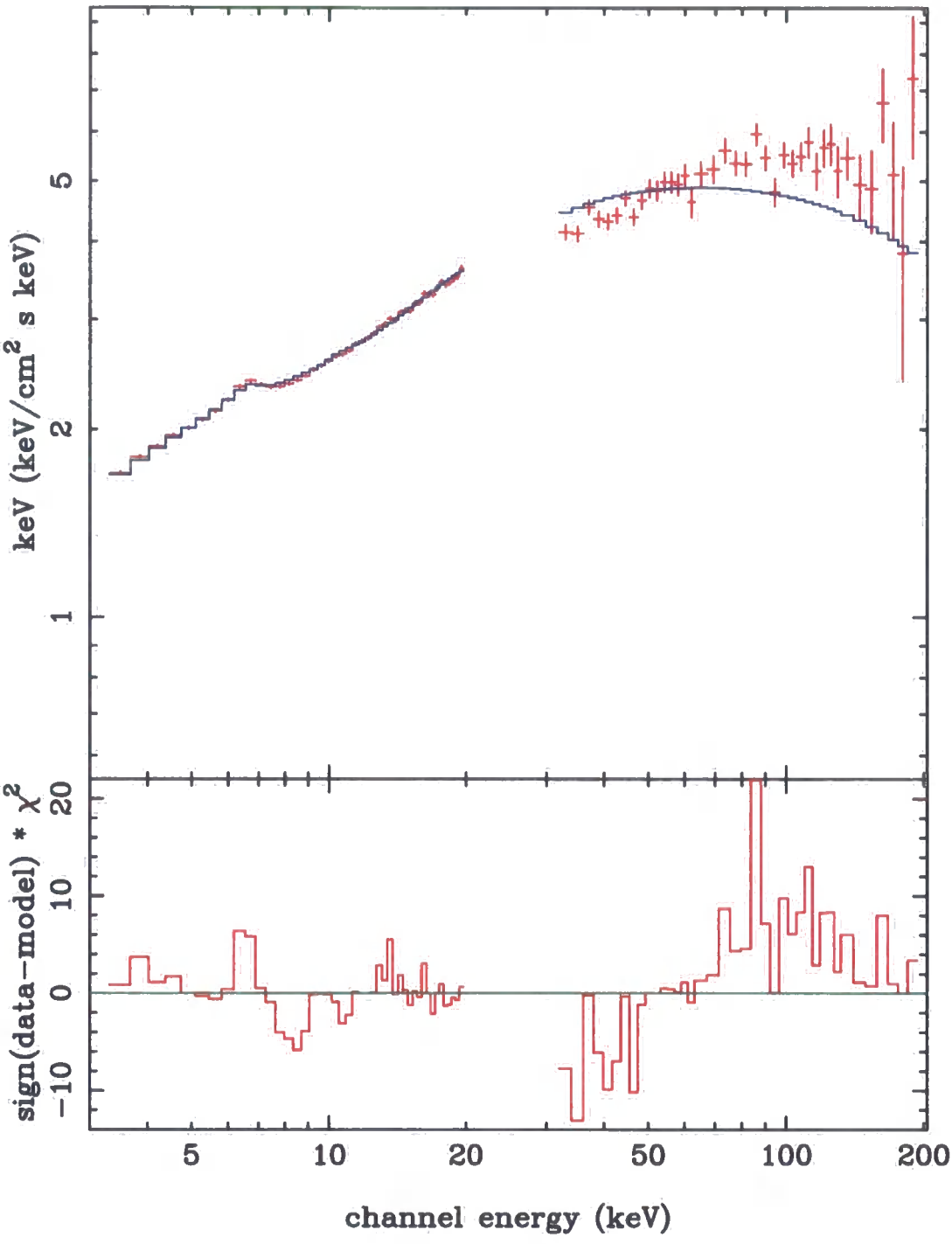

Figure 4.8: As previous figure, but with the XION-FLARE model for reflection from an x-ray illuminated untruncated disc. The large amount of reflection with its rollover at $\sim$ 100 keV means that the slope of the HEXTE spectrum is predicted to be considerably steeper than that of the PCA, while the observed HEXTE data have a rather similar slope.

a disk (Poutanen & Svensson 1996). This approximates the magnetic flare geometry in the limit when the radial size of the flare is much bigger than its height. Any general magnetic flare geometry should give rise to a continuum which is somewhere between the isotropic Comptonised spectrum, and the anisotropic slab (the COMPPS cylinder or hemisphere geometry is more anisotropic than the slab as it assumes only seed photons from below the flare rather than allowing disk photons to also enter through the side of the flare).

We refit the data with the magnetic flare reflection model using this anisotropic slab continuum. This gives an even worse fit than before, with $\chi^2 = 531/78$, where the continuum has $\tau \sim 1$ and $kT_e = 85$ keV. The reason the fit is so poor is that the seed photon anisotropy leads to a break in the spectrum, such that the low energy spectrum is harder than the high energy spectrum (Haardt & Maraschi 1993; Haardt et al. 1993). The low energy spectrum then predicts even less high energy emission than for isotropic seed photons. Fig. 4.9 shows the unfolded spectrum and residuals from this model.

The energy at which the anisotropy break occurs depends on the seed photon temperature (Haardt & Maraschi 1993), and the strength of the break will depend on the detailed geometry of the flare (its radius to height ratio) but qualitatively *any* hot plasma illuminated from below produces a continuum which is anisotropic in the sense that there is a steepening of the high energy spectrum as seen by an observer. The limit where this break is below the PCA bandpass requires an uncomfortably low disk temperature of ≤ 10 eV, and leads to the same poor fit as obtained for isotropic seed photons with magnetic flare reflection ($\chi^2 = 259/78$).

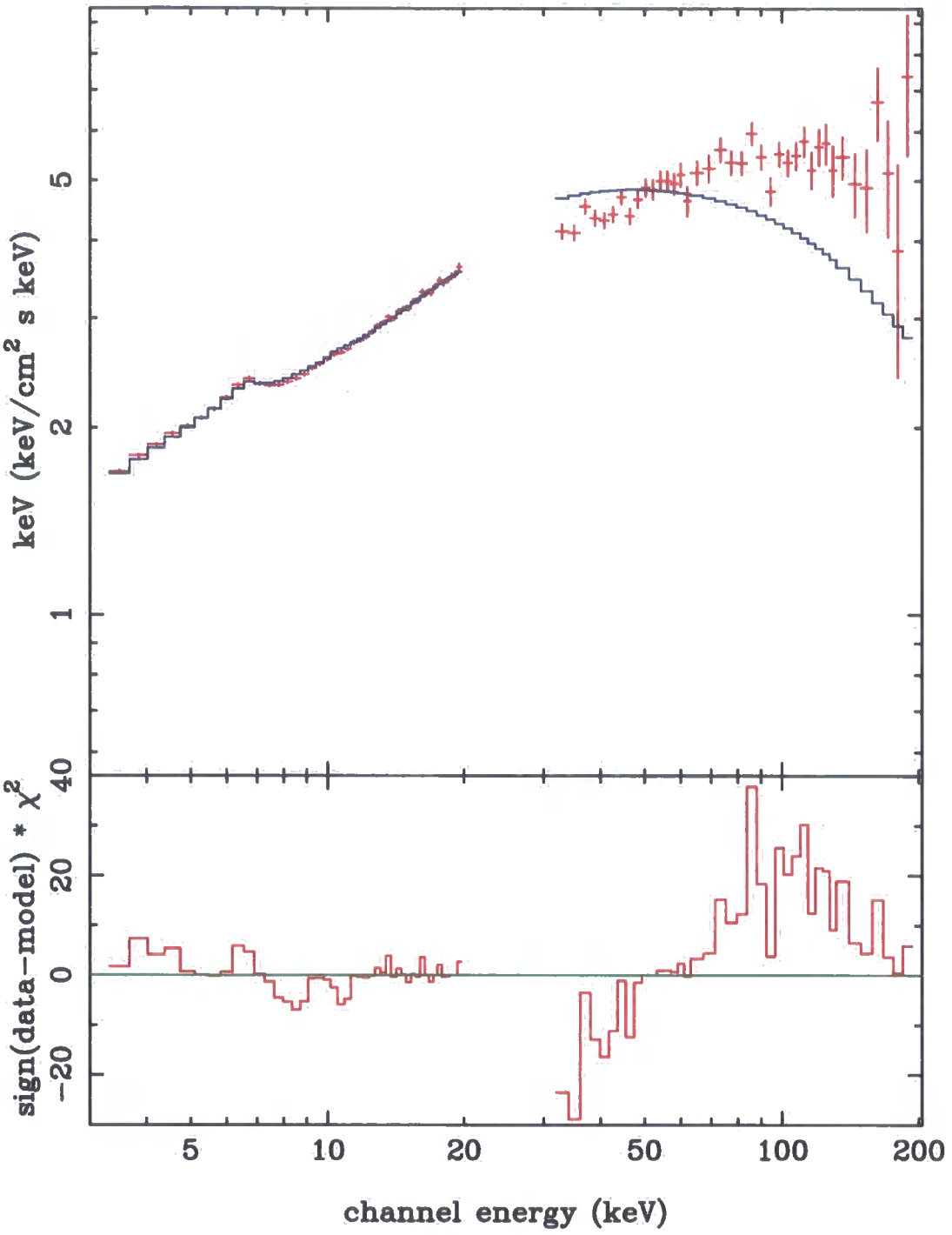

Figure 4.9: As for fig. 3 (reflection from XION-FLARE), but with the anisotropic Compton continuum expected from x-ray emission regions above an accretion disc. The fit is even worse than for isotropic emission as the Compton continuum has a break to a steeper spectrum at high energies due to the anisotropic illumination of the seed photons from the accretion disc. Note the change in scale for the χ^2 panel compared to figs. 2 and 3.

Chapter 5

Discussion & Conclusions

Nature is wont to hide herself.

Heraclitus

The data clearly show that the $2-20keV$ spectrum from the low/hard state of Cyg X-1 does *not* contain a large fraction of highly ionized reflection. This rules out models which have static magnetic flares above an untruncated disc unless the flares have a spectrum which is much harder than that predicted by a single temperature Comptonization model.

Similar conclusions were independently reached by Maccarone & Coppi (2002) from fits to the Cyg X-1 broad-band spectrum. However, they approximated the reflection from magnetic flares by highly ionized, single zone reflection models rather than the full complex ionization reflection models used here. Here we are able to show explicitly that the complex ionization magnetic flare models do not fit the high energy spectrum, while the truncated disc models do.

One way to get some spectral hardening which is expected in a magnetic flare geometry but is neglected in our modelling is for the flares to comptonize some fraction of the reflected photons. The reflected photons are from the disc, so are intercepted by the hot electrons in the flares in the same way as the soft seed photons, and are Compton upscattered to form a hard continuum. With flares covering most of the disc then this can make a 50 – 100 per cent increase to the flux at $200keV$ (Petrucci et al. 2001). A covering fraction of unity for the flares (slab corona geometry) is normally ruled out for the low/hard spectra as this produces many non-reflected, thermalized photons from the hard X-ray illumination. These are also Comptonized by the corona, leading to spectral indices which are too soft to explain the low/hard state (Pietrini & Krolik 1995; Stern et al. 1995; Zdziarski et al. 1998). However, a covering fraction of ~ 0.5 might give enough

Compton scattering of reflection to produce the required ~ 50 per cent excess emission at 200 keV, while also allowing enough seed photons to escape to produce the required hard continuum.

The problems that the magnetic flare models have in matching the high energy flux are exacerbated by the anisotropy break which should be present in the continuum in this assumed geometry, but which has never been convincingly observed (Gierliński et al. 1999). If the magnetic flares are to fit the high energy data then the anisotropy break must be hidden by having a multiple temperature Comptonised continuum. At some level there *must* be a distribution of electron temperatures: it is almost inconceivable that a single temperature distribution can be maintained, especially as the sources are variable so the flare spectra probably evolve with time (e.g. Poutanen & Fabian 1999). A multiple temperature continuum gives another way to boost the high energy flux so that we do not necessarily need to strongly Comptonise the reflected continuum. However, it still seems somewhat contrived that a combined complex continuum plus complex ionization reflection spectrum should so precisely mimic a simple single temperature continuum, truncated disc reflection.

By contrast, a truncated disc/hot inner flow geometry at low mass accretion rates is compatible with the observed hard continuum, lack of anisotropy break, low amount of reflection and relativistic smearing. It can also explain the low temperature and luminosity of the direct emission from the disc (e.g. Esin et al. 2000). This geometry can also give a qualitative explanation for a range of observed correlations if the truncation radius decreases with increasing (average) mass accretion rate. The disc penetrates further into the hot flow, increasing the seed photon flux intercepted by the hot inner flow, leading to a softer continuum spectra. This changing geometry gives a larger solid angle subtended by the disc, leading to an increasing amount of reflection (Poutanen Krolik & Ryde 1997; Zdziarski et al. 1999; Gilfanov et al. 1999; 2000), and relativistic smearing (Życki et al. 1999; Gilfanov et al. 2000; Lubiński & Zdziarski 2001). The variability power spectra are also affected as they contain characteristic frequencies which are most probably linked to the inner edge of the disc, so this can explain the correlated increase in break and quasi-periodic oscillation frequency (e.g. the review by van der Klis 2000; Churazov, Gilfanov & Revnivtsev 2001). Lastly, the collapse of an inner hot flow when it becomes optically thick gives a physical mechanism for the state transition (Esin McClintock & Narayan 1997). The caveats are only that the truncation mechanism and hot flow structure are not well understood theoretically, and that there are quantitative problems in reproducing the correlation between the amount of reflection and spectral shape (Beloborodov 2001).

Thus, if one were to choose between relatively straightforward models, then the trun-

cated disk is definitely favored by our analysis while the magnetic flare model is ruled out. However, the straightforward solutions may be too simple to describe the complexity of accretion disk structure near the black hole. The role and magnitude of secondary effects (Comptonization of the reflection component; multi-temperature nature of flares) not taken into account in our modelling needs to be clarified in the future with detailed calculations.

Bibliography

Arnaud, K.A., George, I.M., Tennant, A.F., 1992. Legacy, 2, 65.

Arnaud K. A., 1996, in Jacoby G. H., Barnes J., eds., Astronomical Data Analysis Software and Systems V. ASP Conf. Series Vol. 101, San Francisco, p. 17

Balbus S.A., Hawley J.A., 2002, Turbulence and Magnetic Fields in Astrophysics," eds. E. Falgarone and T. Passot (astro-ph/0203353)

Ballantyne D., Ross R., Fabian A. C., 2001, MNRAS, 327, 10

Balucinska-Church M., Belloni T., Church M.J., Hasinger G., 1995, A&A, 302, L5

Barrio E., Done C., Nayakshin S., 2003, MNRAS, Accepted.

Beloborodov A. M. 1999, ApJ, 510, L123

Beloborodov A. M. Adv. Sp. Res., 28, 411 (astro-ph/0103320)

Chen X., Abramowicz M.A., Lasota J.-P., Narayan R., Yi I., 1995, ApJ, 443, L61

Churazov E., Gilfanov M., Revnivtsev M., 2001, MNRAS, 321, 759

Collin S., Coupé S., Dumont A.-M., Petrucci P.-O., Różańska A., 2003, A& A, in press (astro-ph/0212528)

Di Salvo T., Done C., Życki P. T., Burderi L., & Robba N. R., 2001, ApJ, 547, 1024

Done C., Nayakshin S., 2001a, ApJ, 546, 419

Done C., Nayakshin S., 2001b, MNRAS, 328, 616

Done C., Życki P.T., 1999, MNRAS, 305, 457

Done C., Madejski G.M., Życki P.T., 2000, ApJ, 536, 213

Done C., Mulchaey J.S., Mushotzky R.F., Arnaud K.A., 1992, ApJ, 395, 275

Ebisawa K., Ueda Y., Inoue H., Tanaka Y., White, N. E., 1996, ApJ, 467, 419

Esin A. A., McClintock J. E., Narayan R., 1997, ApJ, 489, 865

Esin A.A., Kuulkers E., McClintock J.E., Narayan R., 2000, ApJ, 532, 1069

Fabian A.C., Rees M.J., Stella L., White, N.E. 1989, MNRAS, 238, 729

Fabian A.C., Iwasawa K., Reynolds C.S., Young A.J., 2000, PASP, 112, 1145

Field G. B., 1965, ApJ, 142, 431

Fryer C. L., Kalogera V., ApJ, 554, 548-560.

Gierliński M., Zdziarski A. A., Done C., Johnson W. N., Ebisawa K., Ueda Y., Phlips F. 1997, MNRAS, 288, 958

Gierliński M., Zdziarski A.A., Poutanen J., Coppi P.S., Ebisawa K., Johnson W.N., 1999, MNRAS, 309, 496

Gilfanov M., Churazov E., Revnivtsev M., 1999, A& A, 352, 182

Gilfanov M., Churazov E., Revnivtsev M., 2000, Proc. of 5th Sino-German Workshop on Astrophysics SGSC Conf. Ser., 1 (China Science & Technology Press Beijing), ed. G. Zhao, J. J. Wang, H. M. Qiu, G. Boerner, 114 (astro-ph/0002415)

Haardt F., Maraschi L., 1993, ApJ, 413, 507

Haardt F., Done C., Matt G., Fabian A.C., 1993, ApJ, 411, L95

Hamilton A, 1998 http://casa.colorado.edu/ ajsh/schw.shtml

Hawley, J, 2000, ApJ, 528, 462

Hossenfelder, Sabine; Hofmann, Stefan; Bleicher, Marcus; Stcker, Horst; Physical Review D, vol. 66, Issue 10, id. 101502

Kallman T. R., White N. E., 1989, ApJ, 341, 955

Kormendy, J.; Gebhardt, K. 20th Texas Symposium on relativistic astrophysics, Austin, Texas, 10-15 Decem ber 2000, Melville, NY: American Institute of Physics, 2001, xix, 938 p. AIP conference proceedings, Vol. 586. Edited by J. Craig Wheeler and Hugo Martel, p.363

Ko Y.–K., Kallman T. R., 1994, ApJ, 431, 273

Koji Mukai 2001 http://lheawww.gsfc.nasa.gov/docs/outreach/GWUSpaceAstrophysics /Spring01/lectures/accretion/accretion.html

Krolik J. H., McKee C. F., Tarter C. B., 1981, ApJ, 249, 422

Kubota, A.; Done, C.; Makishima, K. MNRAS, 337, L11.

Lightman A.P., White T.R., 1988, ApJ, 335, 57

Longair M.S., 1981, High Energy Astrophysics, vol 1, Publisher: Cambridge University Press.

Lubiński P., Zdziarski A.A., 2001, MNRAS, 323, 37P

Maccarone T.J., Coppi P.S., 2002, MNRAS, submitted (astro-ph/0204160)

Magdziarz P., Zdziarski A. A., 1995, MNRAS, 273, 837

Miller K.A., Stone J.M., 2000, ApJ., 534, 398

Narayan R., Yi I., 1995, ApJ., 452, 710

Nayakshin S. 2000, ApJ, 534, 718.

Nayakshin S., & Kallman T. R., 2001, ApJ, 546, 406 (NK)

Nayakshin S., Kazanas D., Kallman T.R., 2000, ApJ., 537, 833 (NKK)

Nayakshin S., Kazanas D., 2002, ApJ, 567, 85

Pietrini P., Krolik J. H., 1995, ApJ, 447, 526

Poutanen J., Fabian A.C., 1999, MNRAS, 306, 31

Poutanen J., Krolik J.H., Ryde F., 1997, MNRAS, 292, 21P

Poutanen J., Svensson R., 1996, ApJ, 470, 249

Rybicki G.B., Lightman A.P., 1979, Radiative processes in astrophysics, Publisher: Wiley-Interscience.

Ross R.R., Fabian A.C., 1993, MNRAS, 261, 74

Ross R.R., Fabian A.C., Young A.J., 1999, MNRAS, 306, 461

Różańska A., Czerny B., 1996, 1996, AcA, 46, 233

Różańska A., Czerny B., 2000, A& A, 360, 1170

Shakura N.I., Sunyaev R.A. 1973, A& A, 24, 337

Shapiro S.L., Lightman A.P., Eardley D.M. 1976, ApJ, 204, 187

Sunyaev R., Titarchuk L., 1980, A&A, 86, 121

Stern B.E., Poutanen J., Svensson R., Sikora M., Begelman M.C., 1995, ApJ, 449, 13

Van der Klis M., 2000, ARAA, 38, 717

Wilson C.D., Done C., 2001, MNRAS, 325, 167

Young A.J., Fabian A.C., Ross R.R., Tanaka Y., 2001, MNRAS, 325, 1045

Zdziarski A.A., 1998, MNRAS, 296, L51

Zdziarski A.A., Poutanen J., Mikolajewska J., Gierliński M., Ebisawa K., Johnson W.N., 1998, MNRAS, 301, 435

Zdziarski A.A., Lubiński P., Smith D.A., 1999, MNRAS, 303, 11

Zdziarski A.A., 2000, IAU Symposium 195, Eds H. Martens, S. Tsuruta, & M. A. Weber, eds., ASP, pp. 153 (astro-ph/0001078)

Życki P.T., Done C., Smith D.A., 1997, ApJL, 488, 113

Życki P.T., Done C., Smith D.A., 1998, ApJL, 496,25

Życki P.T., Done C., Smith D.A., 1999, MNRAS, 305, 231

Ustinov College

(Graduate Society)